NASA CR-134802

SINGLE STAGE, LOW NOISE, ADVANCED TECHNOLOGY FAN

VOLUME II STRUCTURAL DESIGN

BY: J.L. SCHOENER, G.R. BLACK AND R.H. ROTH

ADVANCED ENGINEERING AND TECHNOLOGY
PROGRAMS DEPARTMENT
GENERAL ELECTRIC COMPANY
CINCINNATI, OHIO

PREPARED FOR

NATIONAL AERONAUTICS AND SPACE ADMINISTRATION

NASA LEWIS RESEARCH CENTER
CONTRACT NAS 3-16813

1. Report No.	2. Government Accession No.	3. Recipient's Catalog No.
NASA CR-134802		

4. Title and Subtitle	5. Report Date
Single Stage, Low Noise, Advanced Technology Fan, Volume II - Structural Design	March 1976
	6. Performing Organization Code

7. Author(s)	8. Performing Organization Report No.
J.L. Schoener, G.R. Black, and R.H. Roth	R76AEG258
	10. Work Unit No.

9. Performing Organization Name and Address	11. Contract or Grant No.
General Electric Company Advanced Engineering and Technology Programs Department Aircraft Engine Group Evendale, Ohio 45215	NAS3-16813
	13. Type of Report and Period Covered
12. Sponsoring Agency Name and Address	Contractor Report
National Aeronautics and Space Administration Washington, D.C. 20546	14. Sponsoring Agency Code

15. Supplementary Notes

Structural Design Report. Project Manager, T.F. Gelder, Fluid System Components Division. Technical Advisor, M.F. Heidmann, V/STOL and Noise Division, NASA-Lewis Research Center, Cleveland, Ohio 44135.

16. Abstract

The structural design for a half-scale fan vehicle, which would have application on an advanced transport aircraft, is described. The single stage advanced technology fan was designed to a pressure ratio of 1.8 at a tip speed of 503 m/sec (1650 ft/sec). This mechanical design report describes the fan rotor design and the design of various structures of the vehicle; eg, stators, casings, splitters, seals, adapters, etc.

This report, entitled Volume II - Structural Design, is one of three in a series of design reports for the advanced technology fan. Other reports in the series include: Volume I - Aerodynamic Design and Volume III - Acoustic Design.

17. Key Words (Suggested by Author(s))	18. Distribution Statement
Airfoil stresses Dovetail stresses Tip shroud stresses Rotor structure stresses Blade variation Blade untwist Structures Vibratory Stresses	Unclassified - Unlimited

19. Security Classif. (of this report)	20. Security Classif. (of this page)	21. No. of Pages	22. Price*
Unclassified	Unclassified	44	

* For sale by the National Technical Information Service, Springfield, Virginia 22151

TABLE OF CONTENTS

LIST OF TABLES

LIST OF ILLUSTRATIONS

LIST OF ILLUSTRATIONS (Concluded)

SECTION I

SUMMARY

A high speed, low noise, high bypass ratio, single stage research fan with two booster stages and a flight-type, variable-geometry inlet has been designed by the General Electric Company under the sponsorship of NASA (Contract No. NAS3-16813). This report, entitled Volume II - Structural Design, is one of three in a series of design reports for the advanced technology fan. It presents the structural design of this low radius ratio fan and booster suitable for an advanced transport aircraft engine. Other reports in this series include: Volume I - Aerodynamic Design and Volume III - Acoustic Design, which are References 1 and 2, respectively.

The fan and booster components are designed in a scale-model flow size convenient for testing with existing facility and vehicle hardware. The 44 medium-high aspect ratio (3.34) blades have an integral tip shroud to provide safe aeromechanical operation at all operating conditions.

The single-stage fan was designed to an average total pressure ratio in the bypass duct downstream of the outlet guide vane of 1.8 at a tip speed of 503 m/sec (1650 ft/sec). Studies of blade vibrational characteristics, i.e., natural frequencies resonance or harmonic conditions, flutter, rotor critical speed and other operational problems, were conducted with the objective of achieving mechanical reliability of the test compressor and associated hardware.

SECTION II

INTRODUCTION

Low noise and exhaust emissions and economical operation are the primary requirements for advanced transport aircraft. The successful development and acceptance of a subsonic, long-range transport for the next generation are greatly dependent upon technological improvements in the areas of fan aerodynamics and acoustic suppression. To help provide this fan technology, the General Electric Company was contracted to design a high speed, low noise, single-stage research fan with two booster stages (hereafter referred to as an advanced technology fan), a variable inlet and an acoustically treated fan exit duct, all applicable for an advanced high bypass, low noise engine. To utilize existing hardware and facilities, the subject fan was designed to be half scale.

Under a separate and earlier contract with NASA (Contract NAS3-15544, References 3 & 4), parametric studies were performed to optimize the engine cycle characteristics for a typical advanced transport aircraft. Based on these studies, plus the current contract Statement of Work, an engine cycle was selected for an advanced transport designed to cruise between 0.85 and 0.90 Mach number. A fan pressure ratio of 1.8 to 1.9 and a bypass ratio of approximately 6:1 were determined to be desirable. Furthermore, it is desirable to raise the pressure ratio of the flow entering the core compressor to about 2.5 to 3.0 by the addition of booster stages. This provides an overall cycle pressure ratio of 30:1 or greater and still uses only a single-stage turbine to drive the high pressure compressor. Fan tip speeds of 488 to 518 m/sec (1600 to 1700 ft/sec) are required to achieve the desired pressure ratio in a single, low radius-ratio stage with adequate stall margin. A high specific flow rate of 215 kg/sec m^2 (44.0 lbm/sec ft^2) was chosen to minimize the fan diameter.

The fan design consists of three basic test configurations: 1) a rear-drive aero vehicle, 2) a rear-drive acoustic vehicle incorporating an acoustic hybrid inlet, and 3) a front-drive acoustic vehicle incorporating an acoustically treated bypass duct containing an acoustically treated splitter. The fan vehicle hardware was designed to mate to the existing contractor facility as illustrated by the interfaces shown on Figure 1. A more detailed view of the new hardware designed under this contract is shown in Figure 2. The advanced technology fan utilizes an existing fan frame, inlet, discharge duct, pedestal support, bearing, sump, and seal system; plus a pair of variable-vane, cascade-type discharge valves which permit independent throttling of the core and the bypass flows.

This volume presents the mechanical/structural design and specification of the new hardware components required for the fan vehicle and is based on the vehicle in the rear-drive, aerodynamic test configuration. Other reports

in this series include Volume I - Aerodynamic Design and Volume III - Acoustic Design, which are References 1 and 2 respectively.

A visual representation of the overall program and report organization is shown on the following page.

DESCRIPTION OF ADVANCED TECHNOLOGY FAN REPORTS

DESIGN REPORTS

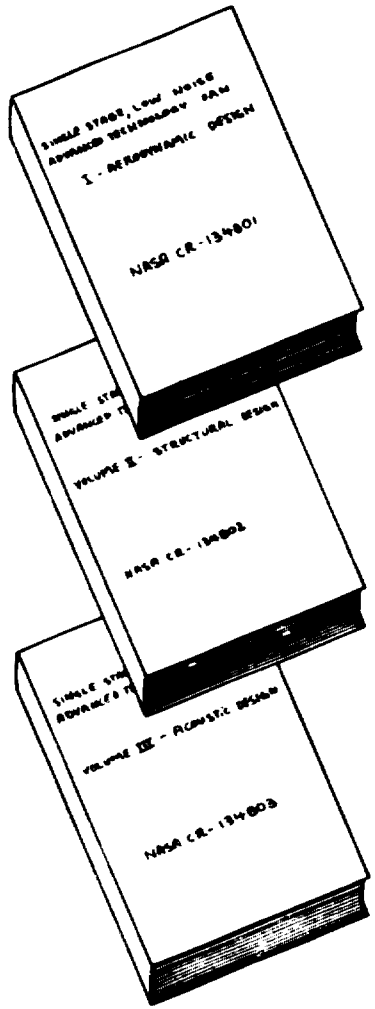

ANALYSIS (FINAL) REPORTS

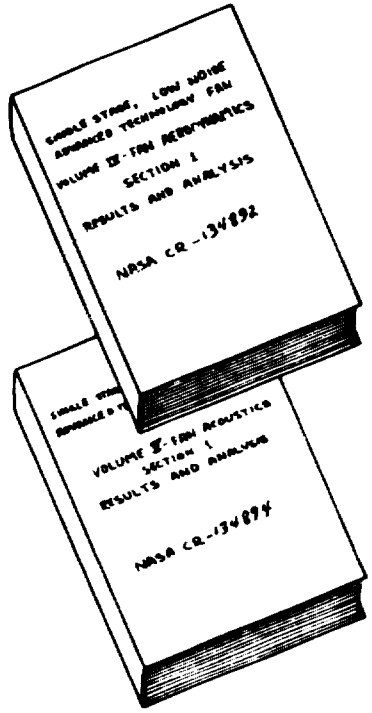

DATA REPORTS

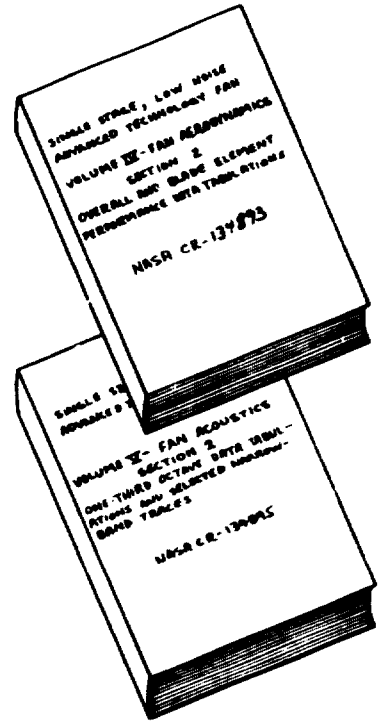

SECTION III

FAN ROTOR MECHANICAL DESIGN

A. Description

The single-stage fan rotor of the advanced technology fan is designed for a high tip speed. The 90.37 cm (35.88 in.) diameter (half-scale size) was chosen in order to be compatible with existing GE test facilities at Peebles, Ohio. The fan blades are tip shrouded and made of titanium 6-6-2. The 100% corrected design speed of the fan rotor is 10,628 rpm. The maximum physical never to be exceeded overspeed was set at 11,692 rpm/110% of the design speed on a standard day. The fan rotor design parameters are presented in Table I, and the fan blade geometric parameters are presented in Table II, below.

Table I. Fan Rotor Blade Design Parameters.

Based on cruise operation at Mach No. = 0.85, altitude 11,000 m (36,089 ft)	
Parameter	Value
100% Design Corrected Rotor Speed	10628 rpm
Corrected Airflow	117.9 kg/sec (259.9 lb/sec)
Corrected Flow per Annulus Area	215 kg/sec-m^2 (44.0 lbs-sec/ft^2)
Bypass Ratio	6.0
Pressure Ratio (Bypass)	1.80
(Core)	1.69
Corrected Tip Speed	503 m/sec (1650 ft/sec)
Inlet Radius Ratio	0.38

Table II. Fan Rotor Blade Geometric Parameters.

Parameter	Value
L.E. Tip Radius	44.7 cm (17.60 in.)
L.E. Hub Radius	18.64 cm (7.34 in.)
Aspect Ratio (Pitch)	3.34
Number of Blades	44
Airfoil Type	Arbitrary
Chord, Root Tip	7.348 cm (2.8931 in.) 9.630 cm (3.7914 in.)
Max. Thickness/Chord Root Tip	0.104 0.0425
Camber Angle, Root Tip	1.4207 rad (81.4°) -0.0243 rad (-1.68°)
Stagger Angle, Root Tip	0.1307 rad (7.49°) 1.1449 rad (65.60°)
Airfoil Edge Dia, Root, L.E. Tip, L.E.	0.4572 mm (0.018 in.) 0.2032 mm (0.008 in.)
Solidity, Root Tip	2.76 1.51
Dovetail Type	Single Tang
Shroud Type	Tip

NOTE: All airfoil dimensions and angles are referenced to a flat surface.

A side view of the rotor blade with dimensions is presented in Figure 3. The radial distribution of rotor blade chords, camber angle, stagger angle, and maximum thickness-to-chord ratio are presented in Figures 4 through 7, respectively.

B. Airfoil Stresses

Steady-state spanwise stresses (stresses parallel to the longitudinal axis of the blade) were determined by a computer program based on beam theory. This program takes into account the cumulative effect of centrifugal and gas loads on the airfoil and the centrifugal load of the tip shroud. The resulting stress distributions along the airfoil at the leading edge, trailing edge, and at the point of maximum section thickness on the convex and concave sides, are plotted in Figure 8.

The spanwise stress distribution along the airfoil root was found using a semiempirical approach referred to as "end-effects" testing. An existing blade whose root geometry was similar to the advanced technology fan blade was subjected to a series of static pull tests. The response of this blade to applied bending moments and spanwise loads was determined from strain-gage readouts. Based on these results, stress functions were constructed that described the blade root stress response to each of the applied loadings (moments and tensile pull). This procedure has been used extensively at General Electric and found to be a reliable method of predicting airfoil root stress response. The loads computed for the blade root were then input to these stress functions to obtain the airfoil root stresses. These stresses are referred to as being corrected for end effects.

The resulting airfoil stress analysis, corrected for end effects and plotted in Figure 9, identifies the maximum steady-state airfoil stress at 100% design speed to be 0.572 GN/m^2 (83 KSI) occurring at the blade root, convex side, near the trailing edge. The maximum stress at 110% design speed was 0.689 GN/m^2 (100 KSI), which is well below the 0.2% yield strength of the material, as listed in Table III.

The stress analysis procedure employed was to calculate stress and deflection distributions at the 100% design point. The stresses occurring at the 110% maximum physical speed condition were then calculated only for the maximum stress points. Figures displaying stress and deflection data in this report present the two items of design interest: 100% design speed stress and deflection patterns, plus 110% design speed maximum stresses.

The airfoil stacking axis was offset 0.091 cm (0.036 in.) from the dovetail centerline in order to reduce the centrifugally induced root moment. This was done in place of tilting the stacking axis, as tilting the airfoil can cause unfavorable bending moments arising from the tip shroud. The stacking axis and all blade coordinates are tabulated in Reference 1.

Table III. Material Properties of Rotor Structure Components.

Characteristic	Ti 6-6-2(1) (Blade)	D6AC Steel (Disk)	17-4 PH Steel (Spinner)	4340 Steel (Shaft)
0.2% Yield Strength at 200° F	1.04 GN/m^2 (151 KSI)	1.30 GN/m^2 (188 KSI)	0.68 GN/m^2 (99 KSI)	0.70 GN/m^2 (101 KSI)
Ultimate Tensile Strength at 200° F	1.10 GN/m^2 (160 KSI)	1.52 GN/m^2 (221 KSI)	0.83 GN/m^2 (121 KSI)	0.87 GN/m^2 (126 KSI)
Allowable Single-Amplitude Alternating Stress for Infinite Life at 200° F and (40 KSI) Mean Stress	0.27 GN/m^2 (39 KSI)	0.51 GN/m^2 (74 KSI)	(Not Required)	
(80 KSI) Mean Stress	0.17 GN/m^2 (25 KSI)	0.41 GN/m^2 (60 KSI)		
(120 KSI) Mean Stress	0.07 GN/m^2 (10 KSI)	0.31 GN/m^2 (46 KSI)		

All properties are General Electric average test values minus three standard deviation units which are then considered to be the minimum acceptable properties.

(1) No modification for section size.

C. Dovetail Stresses

A dovetail shank geometry was chosen providing a good load path transition between the airfoil root and shank. An eight degree (8°) dovetail skew angle, closely approximating the airfoil root stagger angle, was chosen, as shown on the dovetail/shank configuration illustrated in Figure 10.

Dovetail stresses were calculated at six locations on both the blade and disk dovetail (Figure 11). The stresses determined were the "neck" stress (stress due to centrifugal and moment loading on the dovetail neck), "tang" stress (stress arising from loading applied to the flat contact surface), "combined" stress (effective stress computed from the neck and tang stresses), and the "crush" stress (average compressive stress on the flat contact surface). These computations were made using a General Electric computer program employing beam theory and the Heywood deep-beam projection formula based on photoelastic test experience (see Reference 5).

The maximum steady-state combined stress in the blade dovetail was at point 4 and was 0.73 GN/m^2 (106 KSI) at 110% speed. The maximum combined stress in the disk was 0.97 GN/m^2 (140 KSI) at 110% speed. These values are each below 75% of the minimum 0.2% yield strengths, as tabulated in Table IV. The pressure face maximum crush stress is 0.41 GN/m^2 (60.0 KSI) at 110% speed; this level is low enough to prevent deterioration of the contact surface coating material.

The relative sizes of the blade and disk dovetails were optimized in order to satisfy the so-called "weak link" criterion. This criterion requires the disk dovetail to be stronger than the blade dovetail, which should in turn be stronger than the airfoil. Figure 12 shows the relative stress levels in the blade and disk dovetail when the airoil is in a state of stress corresponding to its vibratory endurance limit. The alternating stress in the airfoil is the maximum allowable alternating stress for the given steady-state stress such that the airfoil can withstand an infinite number of cycles of double-amplitude vibration. It can be seen in Figure 12 that when the airfoil is stressed to its endurance limit, the blade dovetail has a 0.03 GN/m^2 (5 KSI) margin for single-amplitude vibratory stress. The disk has the greatest margin, 0.07 GN/m^2 (10 KSI). Thus, the disk has greater margin over vibratory fatigue failure than the blade dovetail, which in turn has a greater margin than the airfoil. The weak link criterion is, therefore, satisfied.

D. Tip Shroud Stresses

Effective stresses were computed for the blade tip shroud using a General Electric three-dimensional finite element computer program based on the well-known eight-noded isoparametric brick element. See Figures 13 and 14 for sketches of the tip-shroud configuration.

Figure 15 shows the shroud stress distribution along the fillet blend between the shroud and airfoil. This region has been determined to be the location of the highest stress in the shroud region. The maximum stress occurring in this area is 0.53 GN/m^2 (77 KSI) at 100% design speed and 0.64 GN/m^2 (93 KSI) at 110% design speed. This is well below the 0.2% yield strength of the materials which are shown on Table III.

Great care was exercised in arriving at a thickness distribution for the tip shroud. This was done to reduce both edge deflections and panel bending stresses caused by centrifugal loading at high speed.

E. Rotor Structure Stresses

Effective stresses were also determined for the rotating structural components of the advanced technology fan rotor system. A computer program based on equations for shells and rings of revolutions was used in these calculations.

A summary of the location and magnitude of maximum calculated stresses in the rotor structure at 100% design speed is presented in Figure 16. A comparison of the stresses at 100% and 110% design speed and the 0.2% yield strengths of the materials is given in Table IV. As can be seen from this table, the rotor structure is low stressed.

Table IV. Comparison of Design Speed Stress Levels Material Property Limits.

Part	Material	Maximum Steady-State Stresses			Material Properties
		Units	100% Speed	110% Speed	0.2% Yield Strength at 367° K
Spinner Nose & Cone	17-4PH Steel	GN/m^2 (KSI)	0.28 (41)	0.34 (50)	0.68 (99)
Rotor disk (excluding dovetail)	D6AC Steel	GN/m^2 (KSI)	0.68 (100)	0.83 (121)	1.30 (188)
Seal	D6AC Steel	GN/m^2 (KSI)	0.50 (73)	0.61 (88)	1.30 (188)
Drive Shaft	4340 Steel	GN/m^2 (KSI)	0.18 (26)	0.22 (32)	0.70 (101)

F. Blade Vibration and Stability

A vibration and stability analysis for the advanced technology fan blade was conducted. Important parameters resulting from this analysis are summarized in Table V.

Table V. Fan Blade Vibratory Characteristics.

Torsional Reduced Velocity Parameter at 100% speed Design Point at 100% speed stall Point	 1.49 1.43
First Flex Frequency at 100% Design Speed	420 Hz
First Torsional Frequency at 100% Design Speed	1240 Hz
Second Flex Frequency at 100% Design Speed	920 Hz
First Flex Frequency Margin Over 2/Rev Excitation-Blade Only @ 100% Speed	18.5%
First Flex Frequency Margin Over 2/Rev Excitation-Blade/Disk System @ 100% Speed	10%

Blade frequencies at various speeds were calculated from a computer program based on beam theory. Frequencies were determined both for the blade fixed to a rigid rim and also for the case of the blade mounted on a flexible rim (i.e., the blade and disk vibrate as a system). The frequencies thus determined were plotted on a Campbell Diagram (Figure 17). The first torsional frequencies were also used to calculate reduced velocities at various speeds.

A major design consideration for the fan blade was that the first flex natural frequency have adequate margin over a 2/Rev excitation at 100% design speed. The blade (rigid rim) natural frequency is calculated to have an 18.5% frequency margin over 2/Rev, while the two-nodal-diameter blade-disk system has 10% margin. The design goal of 10% frequency margin for this parameter was thus achieved.

Another major design consideration was to avoid regions of blade torsional vibration instability. Reduced velocity parameters and incidence angles were plotted (Figure 18) and compared with past test experience. The stall line lies within the range of possible instability considering total General Electric experience with both cantilever and tip-shrouded blades. The normal operating line, however, lies well outside the measured torsional instability boundary for previous tip-shrouded blades.

G. Blade Untwist

Centrifugal loads due to fan rotation and aerodynamic loads cause the blade airfoil to untwist. The blade platforms and tip shrouds lock up while running, so untwist at the blade root and tip is negligible. Neglecting the airfoil section chordwise bending deformation, the maximum untwist occurs at 62% airfoil height where the untwist equals 0.061 rad (3.48°) at 100% design speed. The blade is pretwisted to exactly match the untwist over the entire span at 100% design speed in order to optimize aerodynamic performance.

SECTION IV

STRUCTURES

The outer fan casings and core and bypass vane shrouds of the advanced technology fan were axially split into 180° segments for assembly and disassembly purposes. The rotor tip casing and stationary portion of the core stator hub seal were designed to incorporate rub surfaces consisting of bonded honeycomb filled with an abradable, epoxy/phenolic microballoon mixture. All stator vanes are specified to be machined from 410 stainless steel, a high strength, low cost alloy. The vanes are peened in the root fillet areas for increased vibratory strength. The bypass Outlet Guide Vanes (OGV) and core stator vanes were designed to be adjustable 4° from the nominal vane setting in 2° increments. Chord angle positioning can be maintained by lock plates which are precision fitted to the slabbed vane trunnions. The deswirl vane cascade is a fabricated assembly consisting of individually machined airfoils bonded into outer and inner slotted rings. A listing of the new stator hardware requirements with their selected materials is contained in Table VI.

Similarity of the advanced technology fan with an existing contractor test vehicle eliminated the need for extensive vehicle vibration analysis. The two vehicles would act almost identically. Since the existing fan was tested first, the advanced technology fan would have the added advantage of test data to substantiate the vibrational analysis.

The major structural analysis pertaining to the static parts of a vehicle of this type involves the vane and frame components. Since the frame is an existing item, the vanes were the only component requiring analysis.

Vane cascades were frequency and stress analyzed using the General Electric Twisted Blade Computer Program. The calculated frequencies are shown in the Campbell diagrams of Figures 19, 20, and 21 for the OGV, core stator, and deswirl vane respectively (these frequencies were verified at a later date via bench testing when the vane hardware became physically available). Vane stiffness is normally designed to avoid the first flexural frequency and first torsional frequency from intersecting the blade passing (excitation) frequency (44/rev) within the normal operating range (60% to 100% speed). Figure 19 and 20 indicate that the bypass OGV and core stator conform to this design practice. These requirements have; however, been waived for the deswirl vane (Figure 21). The deswirl vane is a lightly loaded airfoil. Its position aft of a stator cascade and its fixity at both ends indicate small potential excitation energy for this low-response configuration.

Table VI. New Stator Hardware Requirements and Material Selections for the Advanced Technology Fan.

New Component	Material
Vane, OGV	410 Stainless Steel
Vane, Core Stator	410 Stainless Steel
Vane, Deswirl Stator 3	6061-T652 Aluminum
Rotor Case	6061-T652 Aluminum
Duct Case	6061-T652 Aluminum
OGV Case	1010-1020 Low-carbon steel
OGV Shroud	6061-T6 Aluminum
Splitter	1010-1020 Low-carbon steel
Splitter Cover	6061-T6 Aluminum
Ring Adapter	1010-1020 Low-carbon steel
Core Stator Shroud	6060-T652 Aluminum
Stationary Seal	6061-T651 Aluminum
Core Casing	6061-T652 Aluminum
Deswirl Vane Casings	1010-1020 Low-carbon steel
Frame Adapters	6061-T6 Aluminum
Vane Locking Plates	316 Stainless Steel
Hardwall Panels	6061-T651 Aluminum

The Campbell diagrams on Figures 19, 20, and 21 also indicate several higher order natural frequencies which occur below the blade passing frequency at 110% fan speed. These natural frequencies are identified on the figures by their frequency only, with no reference to their mode shape. The complex mode shapes of these higher order frequencies makes them difficult to define by their vibrational mode.

The Reduced Velocity Parameter has been calculated for each of the three vane cascades to ensure stable operation. Figure 22 shows that the entire operating envelope of the system is well within the region of torsional stability. The stability boundaries shown on Figure 22 have been experimentally established. The torsional stability diagram indicates an adequate incidence angle or stability margin for all three vane cascades.

Figures 23, 24, and 25 are plots of the calculated steady-state airfoil stresses due to air loading for the OGV, core stator, and deswirl vane, respectively. The bypass OGV and core stator stress plots of Figures 23 and 24 show distributions for both cantilevered and fixed-shrouded end conditions.

The trunnion attachment at the inside of the vane is actually somewhere between these two end conditions. For this reason, the vane was analyzed for both end conditions. (When vibratory stress limits were subsequently determined, both stress distributions were factored into the calculations).

The Goodman diagrams of Figure 26 identify the resulting vibratory allowable stresses (these values were subsequently used in conjunction with the vibratory stress distributions acquired during bench testing to establish the vibratory stress limits to use during fan testing). The conclusion reached from the Goodman diagrams is that all three cascades have sufficiently low steady-state stresses to maintain an adequate vibratory margin.

In addition to the previously stated design criteria, other normal design practices have been considered in the configuration of the vane hardware. The trunnions of the vanes have been made stronger than the airfoils, also the fillet radii at the junctions of the airfoils with the vane bases will be of sufficient magnitude to limit the resulting stress concentration factor to 1.5.

SECTION V

RESUMÉ

The structural design for a half-scale fan vehicle which would have application on an advanced transport aircraft is described. The single-stage, low noise, advanced technology fan was designed to a pressure ratio of 1.8 at a tip speed of 503 m/sec (1650 ft/sec).

The fan blades meet flight-type design criteria, as verified by using a computer program for twisted beam analysis. These criteria include first flex frequency margin, instability margin, overspeed stress margin, and satisfaction of the "weak-link" criteria for the disk/blade system.

The ability of the blade design to meet these requirements and remain lightweight is due to the excellent mechanical properties of the titanium 6-6-2 material chosen, and to the significant advantages of using a tip shroud to raise the natural frequencies of a lightweight airfoil.

The disk, spinner parts, and shafting designs were analyzed and found to have more than adequate design margin.

The major structural component, the frame, existed from a previous contract program, eliminating the need for an extensive vehicle vibration analysis. The stator vanes were analyzed, however, according to standard General Electric Design Practices and were found to possess no limitations which would restrict the vehicle's operation.

APPENDIX A

LIST OF SYMBOLS AND NOMENCLATURE

Symbol	Description
C	Vane Cord
F_{1T}	First Torsional Natural Frequency
GN/m^2	Giganewton/Meter^2
i	Incidence Angle
KSI	Thousand Pounds per Square Inch
L.E.	Leading Edge
N/m^2	Newton/Meter^2
/Rev	Per One Revolution
rpm	Revolution per Minute
Ti	Titanium
T.E.	Trailing Edge
V_{Rel}	Relative Velocity
Y.S.	Yield Strength
N_f	Fan Speed

REFERENCES

1. Sullivan, T.J., Younghans, J.L., and Little, D.R., "Single Stage, Low Noise, Advanced Technology Fan, Volume I - Aerodynamic Design," NASA CR-134801, March, 1976.

2. Kazin, S.B. and Mishler, R.B., "Single Stage, Low Noise, Advanced Technology Fan, Volume III - Acoustic Design," NASA CR-134803, March, 1976.

3. Compagnon, M.A., "Propulsion System Studies for an Advanced High Subsonic, Long Range Jet Commercial Transport Aircraft," NASA CR-121016, November, 1972.

4. "Studies for Determining the Optimum Propulsion System Characteristics For Use in a Long-Range Transport Aircraft Comprehensive Data Report," NASA Contract NAS3-15544, June, 1972.

5. Roark, R.J., "Formulas for Stress and Strain," 4th ed. McGraw-Hill, 1965 pp. 131-132.

ILLUSTRATIONS

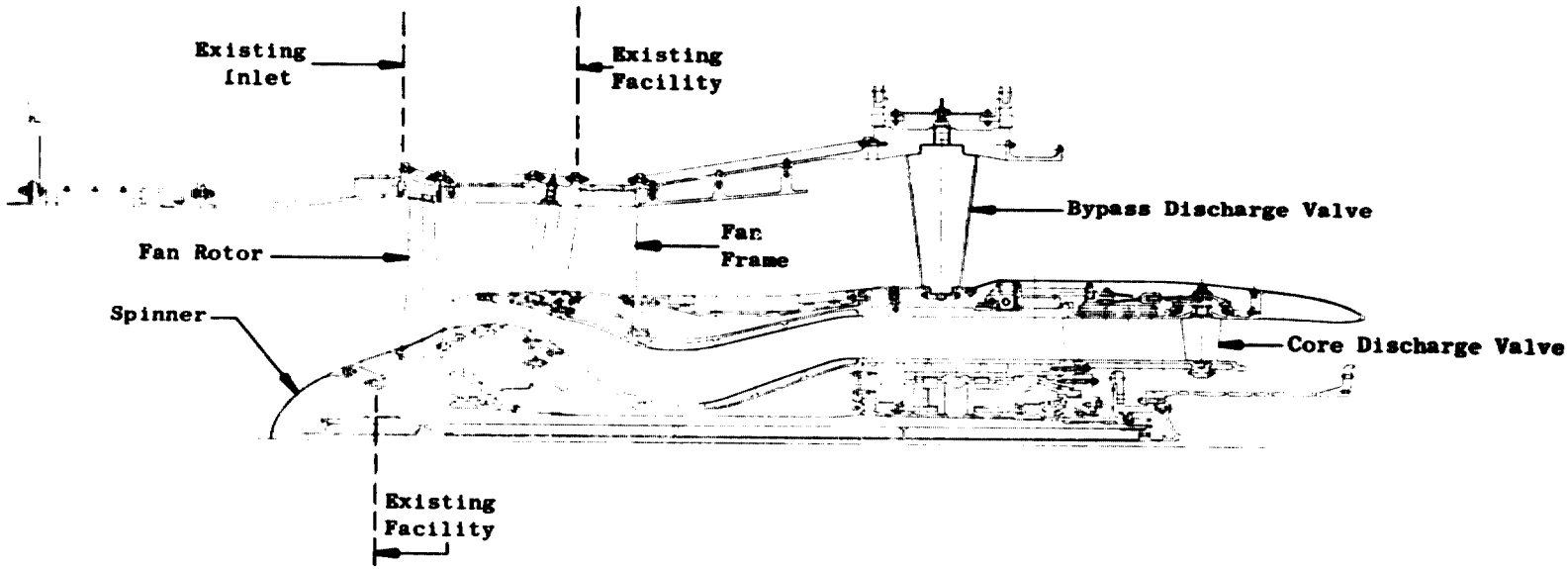

Figure 1. Advanced Technology Fan Vehicle Assembled to the Test Facility.

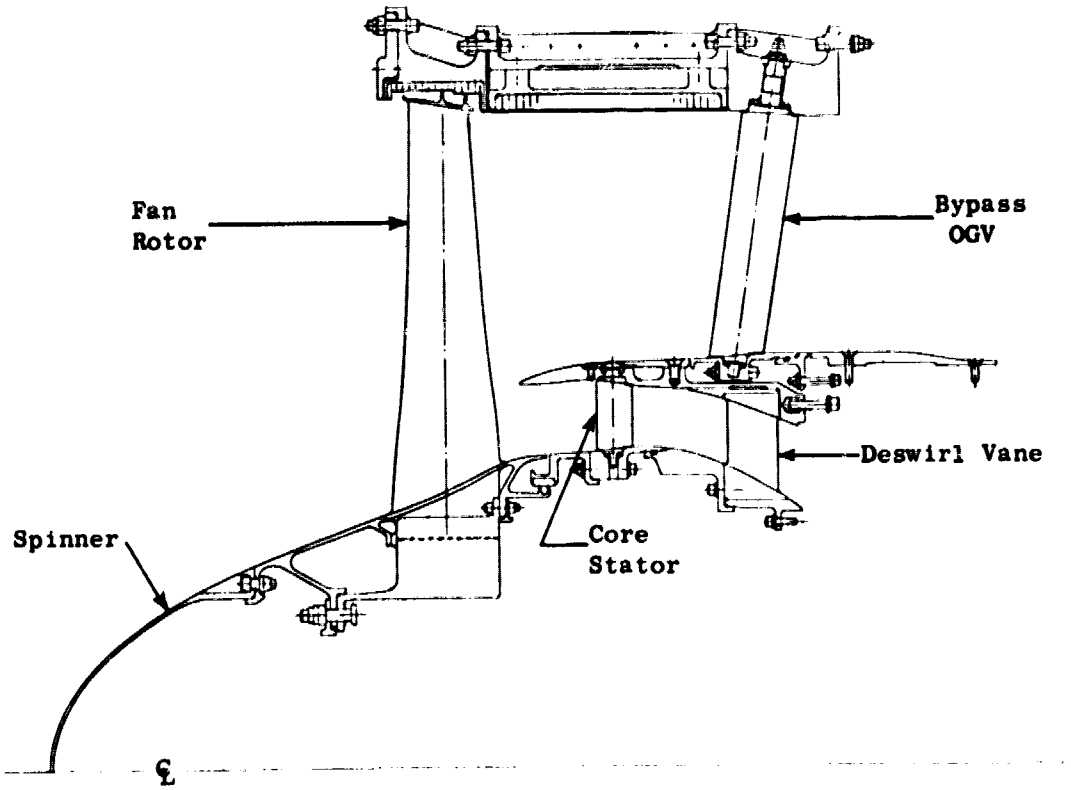

Figure 2. Advanced Technology Fan Vehicle Showing New Hardware Required.

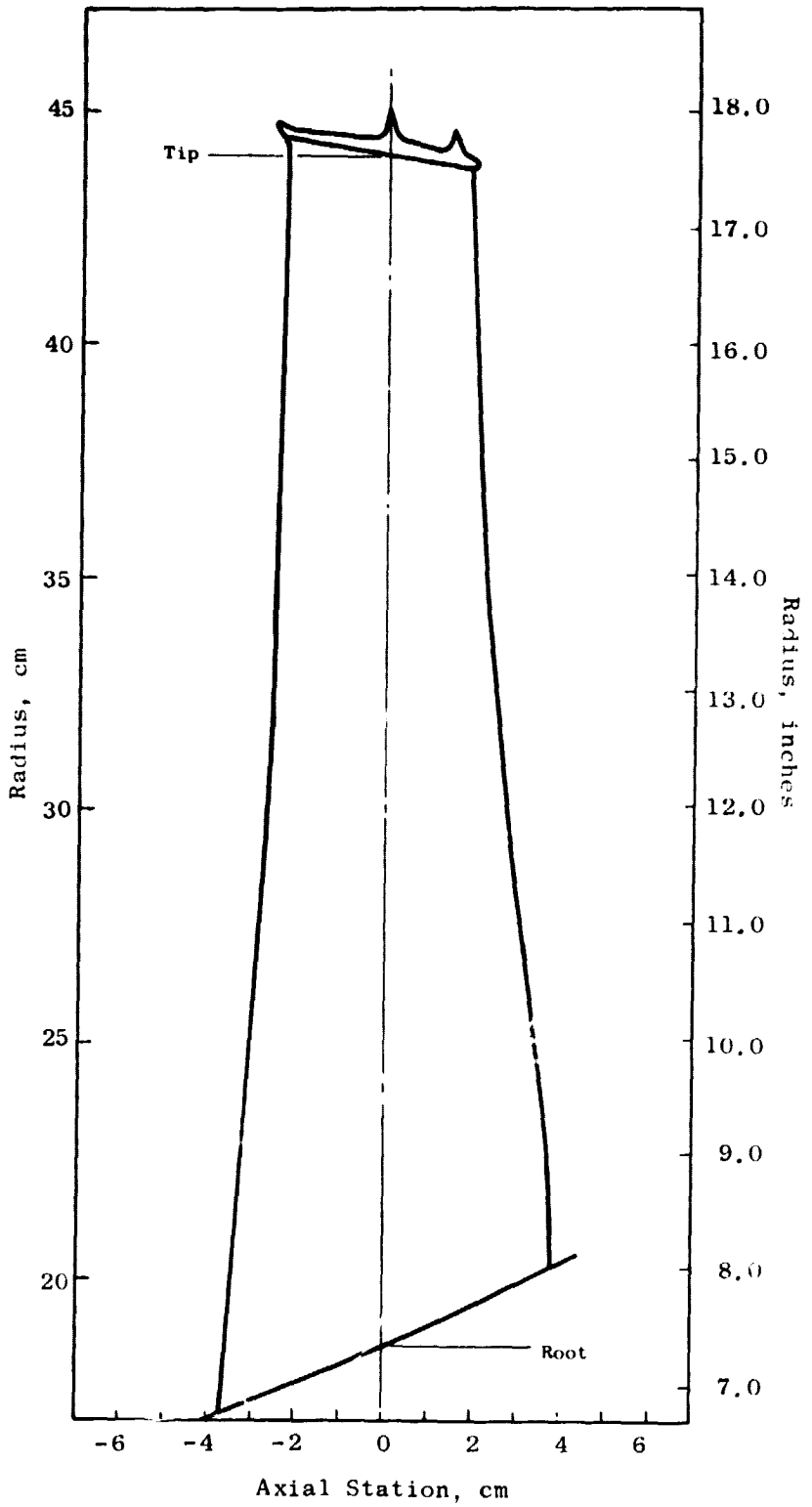

Figure 3. Fan Rotor Blade Geometry.

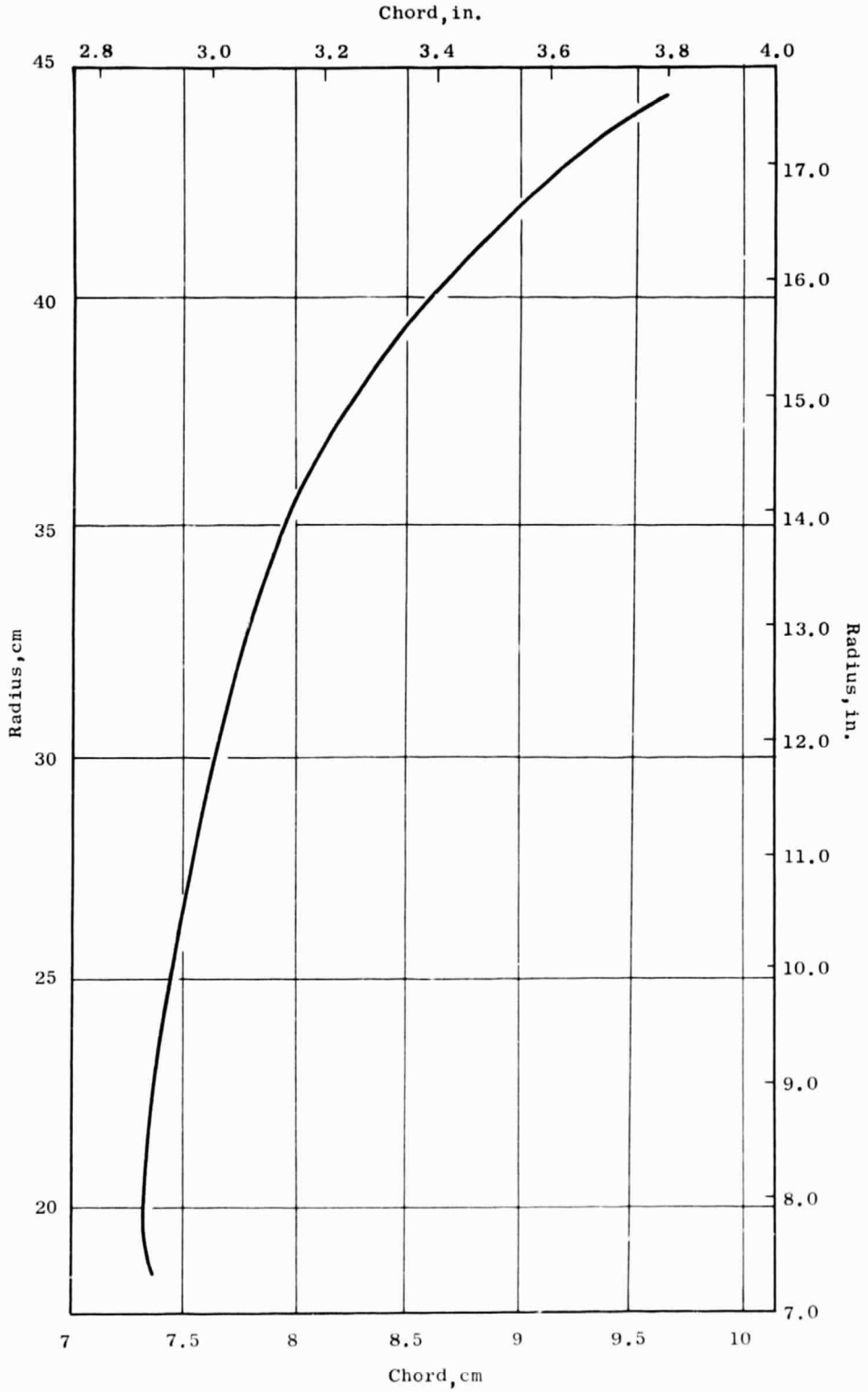

Figure 4. Fan Rotor Blade - Blade Chord Vs. Radius.

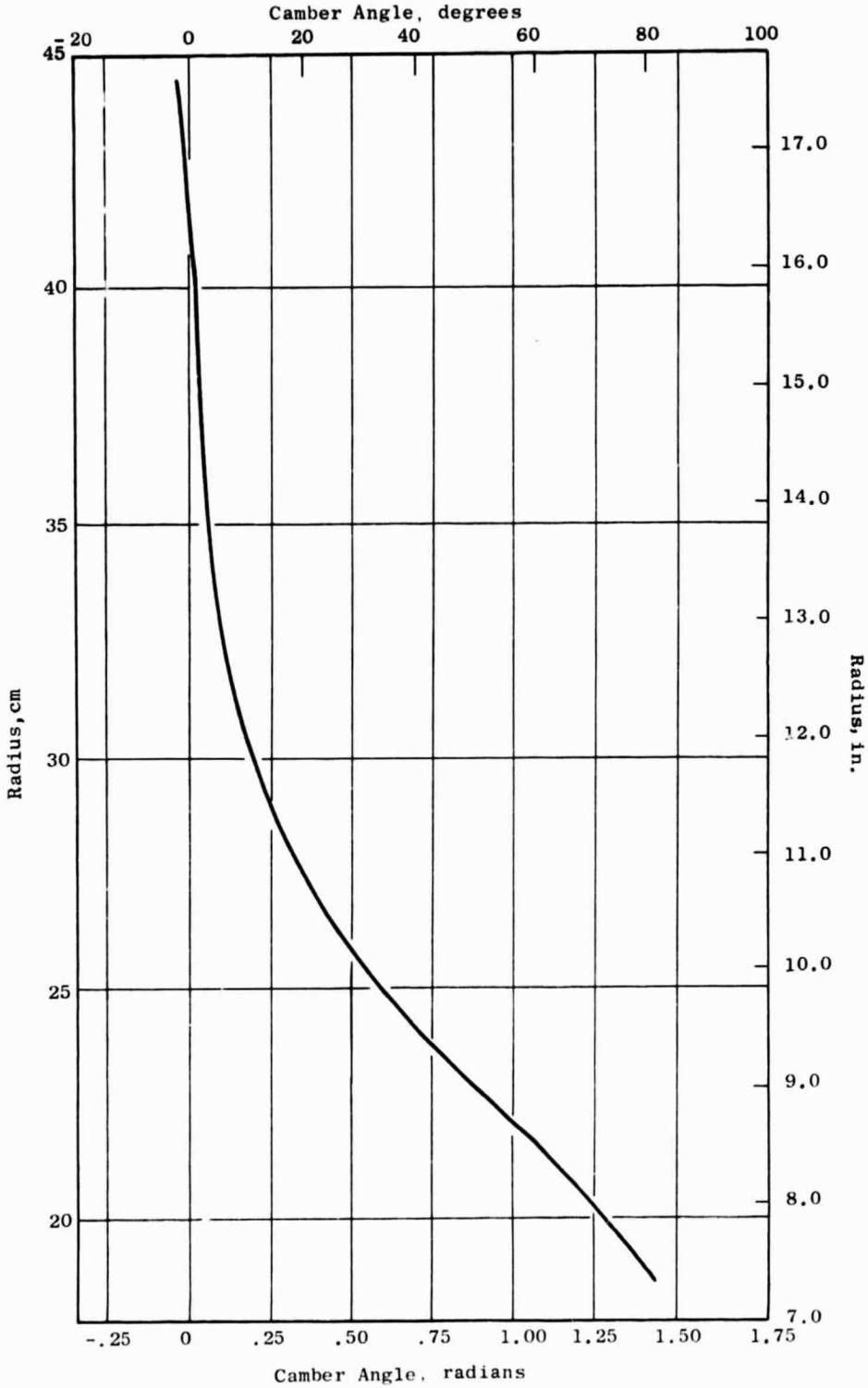

Figure 5. Fan Rotor Blade - Camber Angle Vs. Radius.

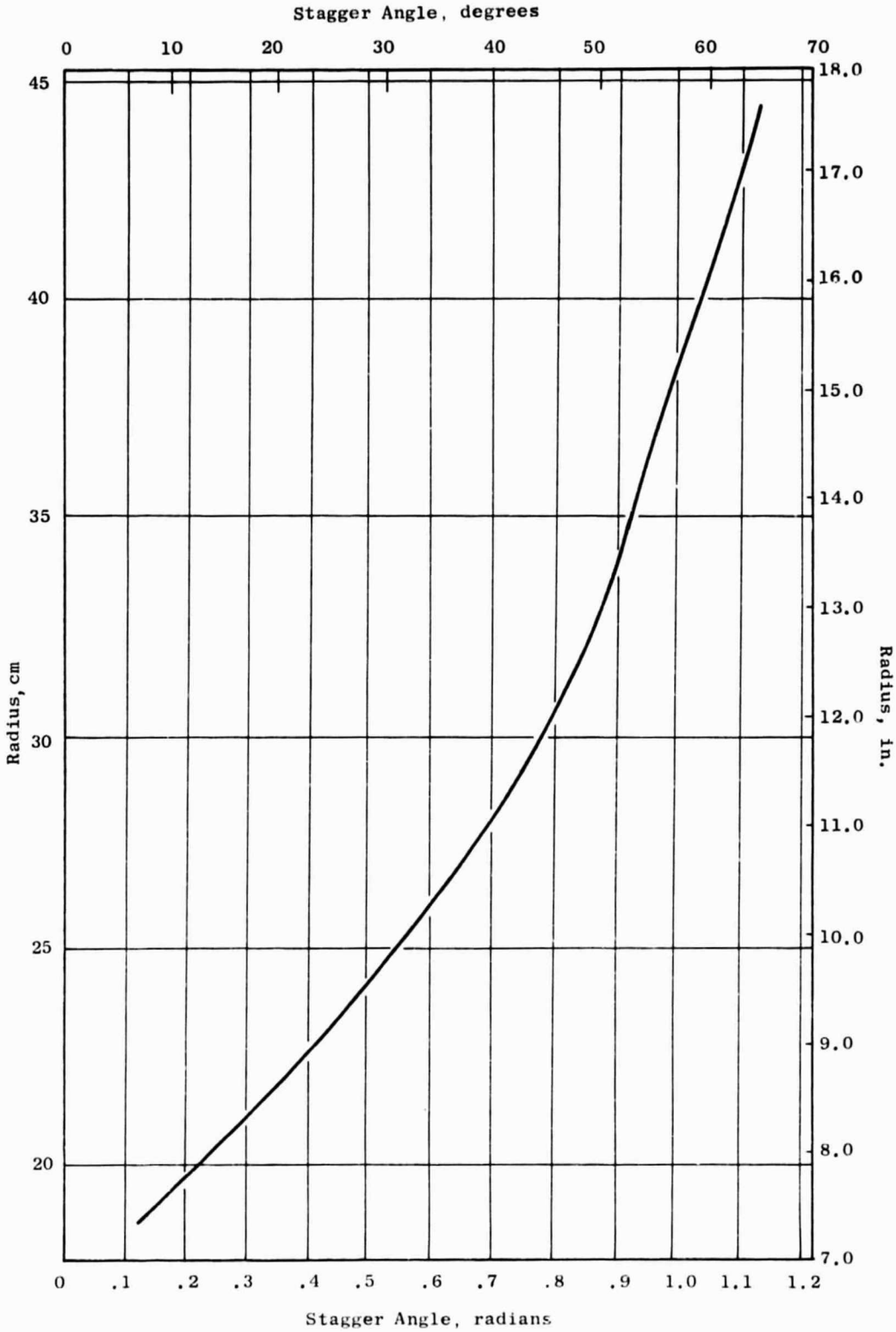

Figure 6. Fan Rotor Blade - Stagger Angle Vs. Radius.

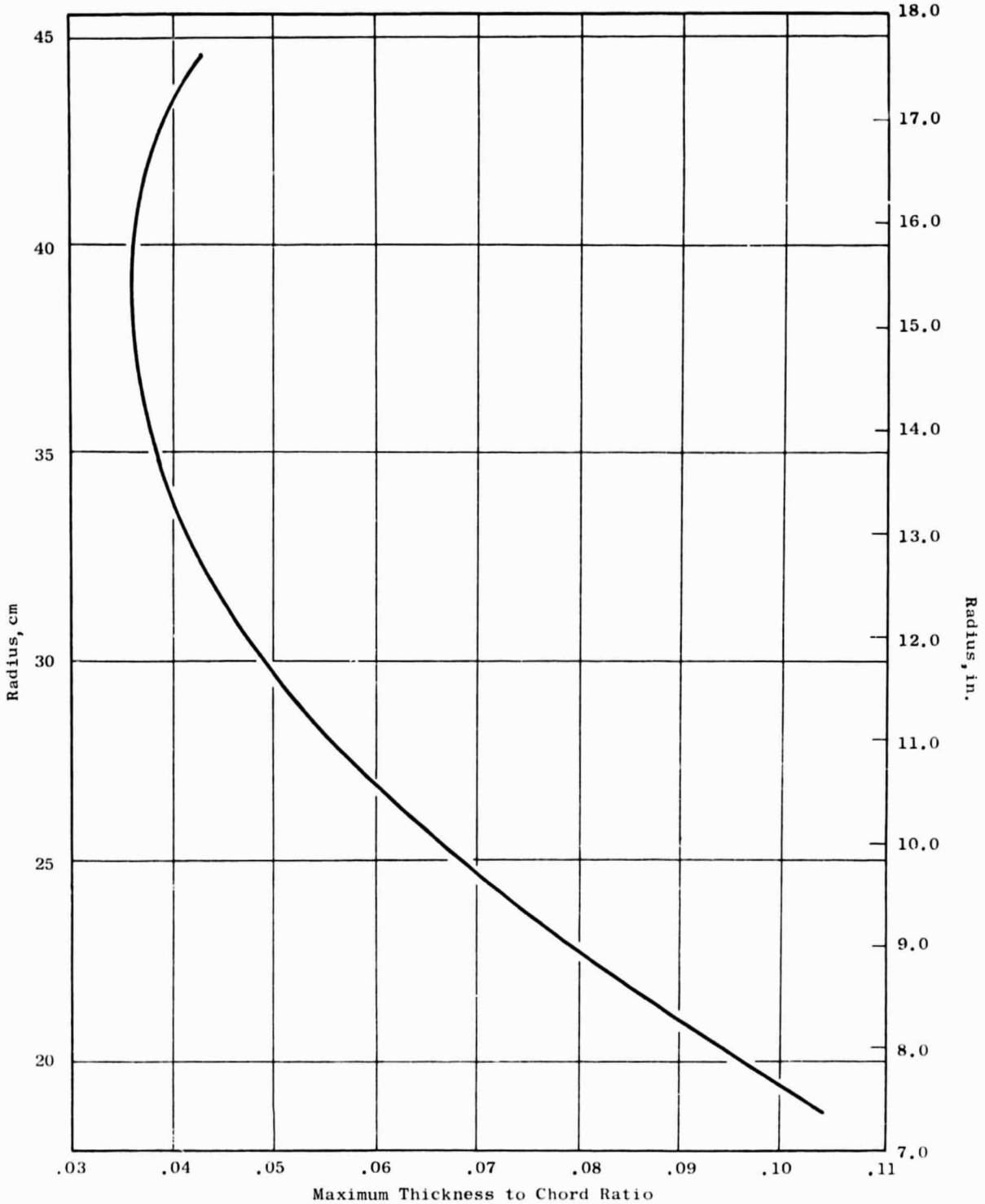

Figure 7. Fan Rotor Blade - Maximum Thickness to Chord Ratio Vs. Radius.

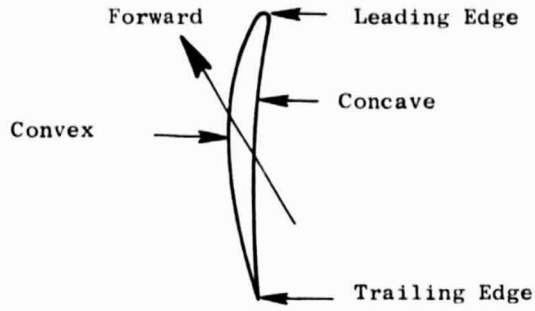

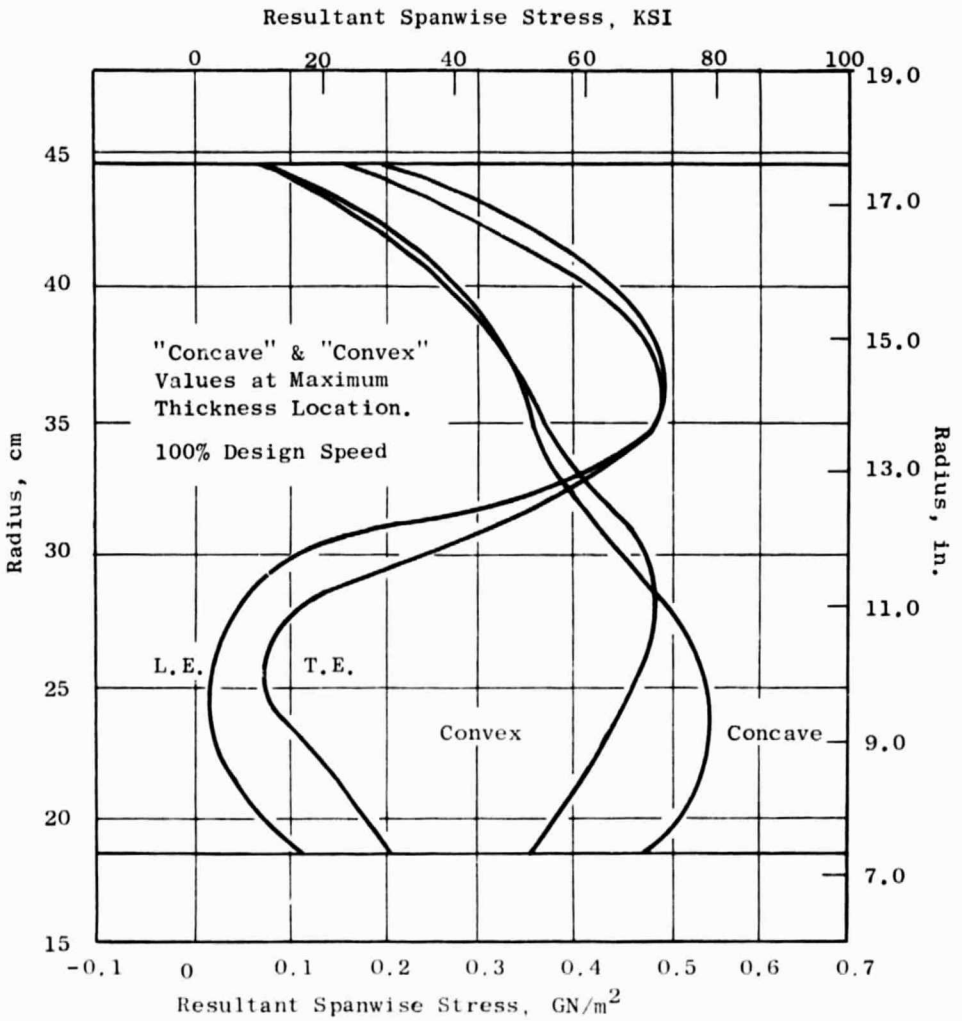

Figure 8. Airfoil Resultant Spanwise Stress Distribution at 100% Design Speed (Uncorrected Beam Theory).

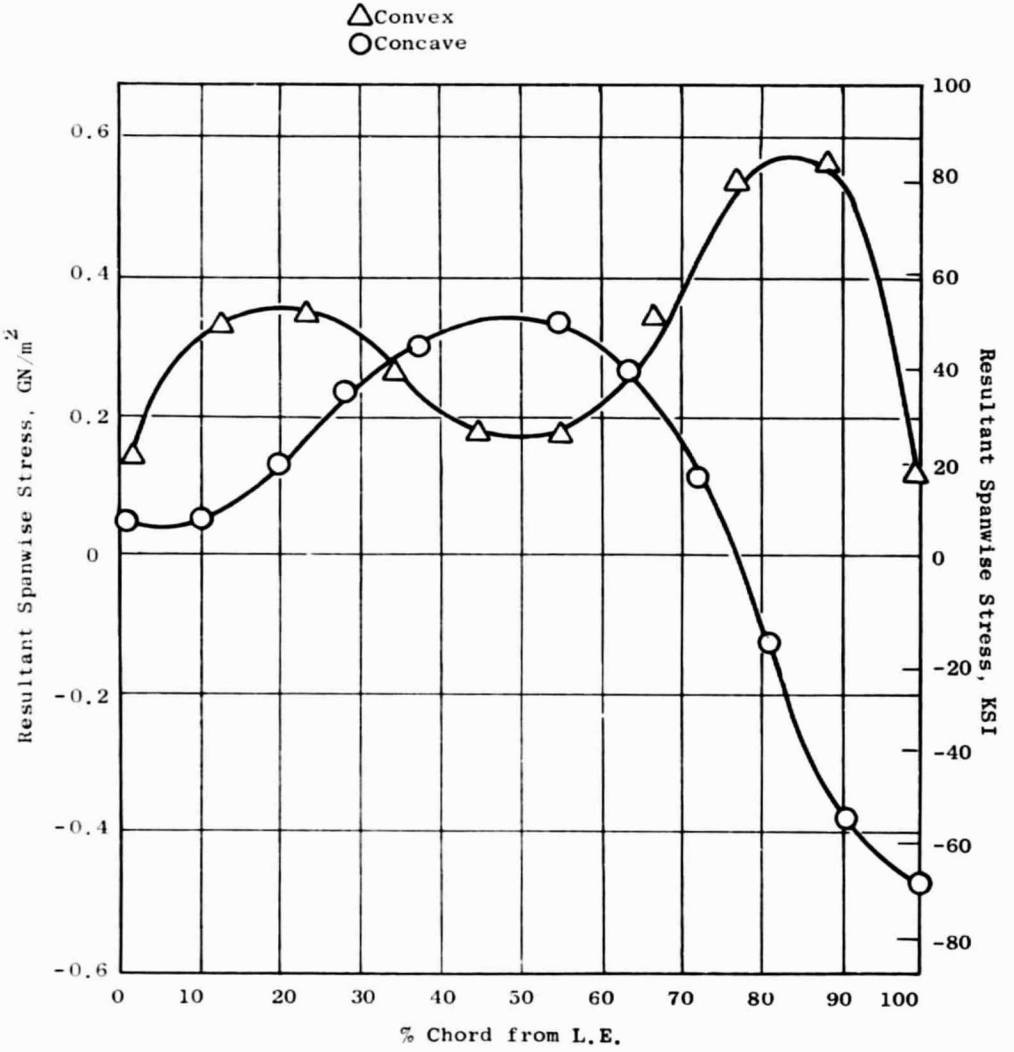

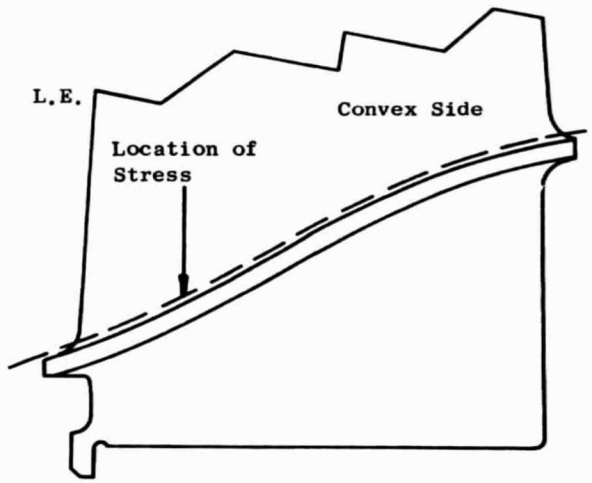

Figure 9. Fan Rotor Blade - Root End Effect Stress, 100% Design Speed.

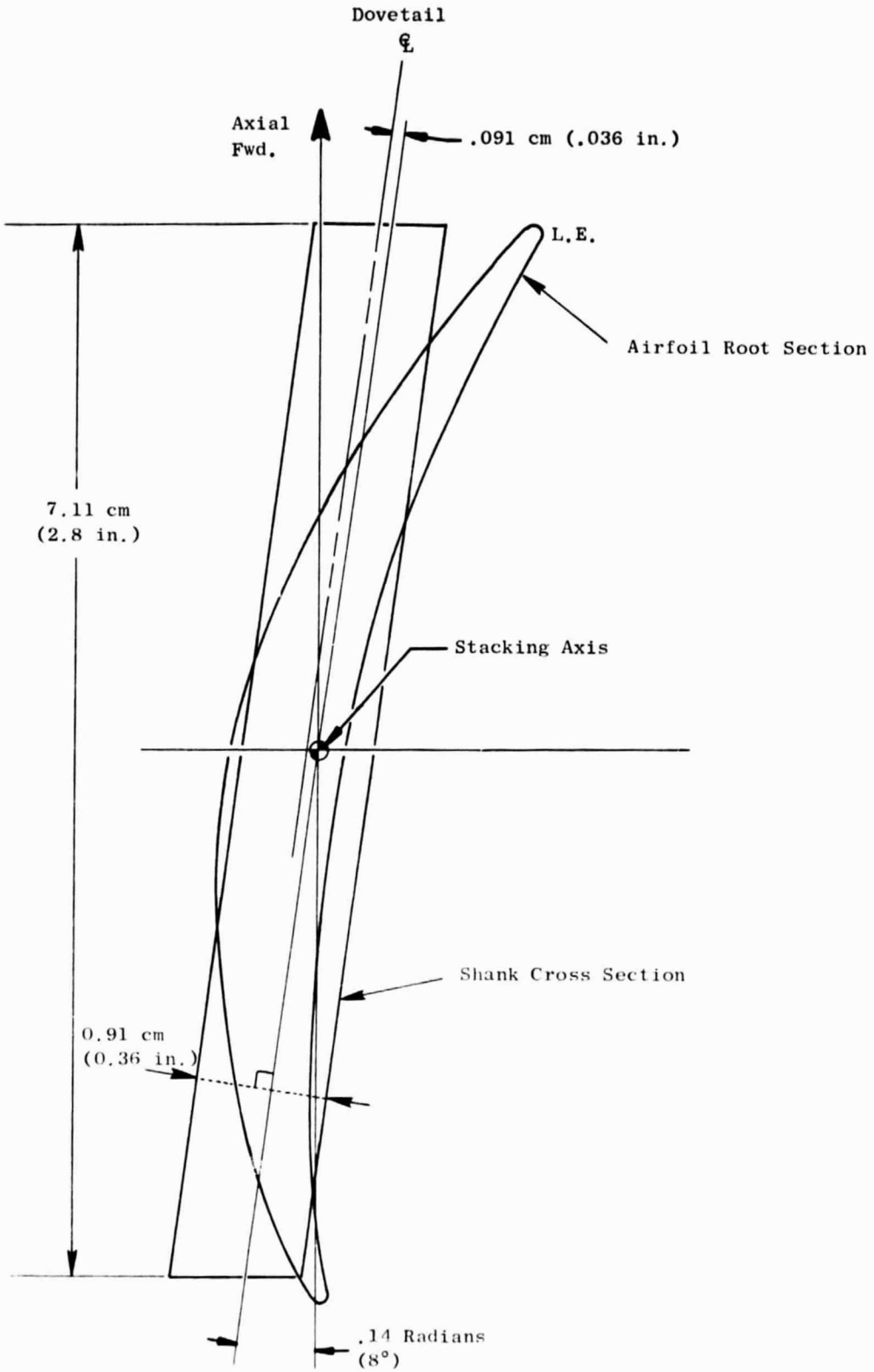

Figure 10. Fan Rotor Blade - Airfoil Root Section/ Dovetail Shank Alignment.

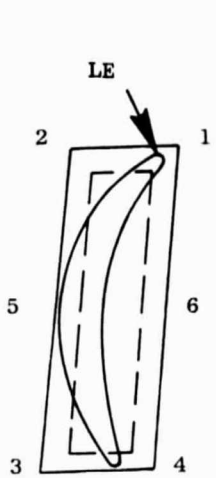

Key to Different Calculation Points

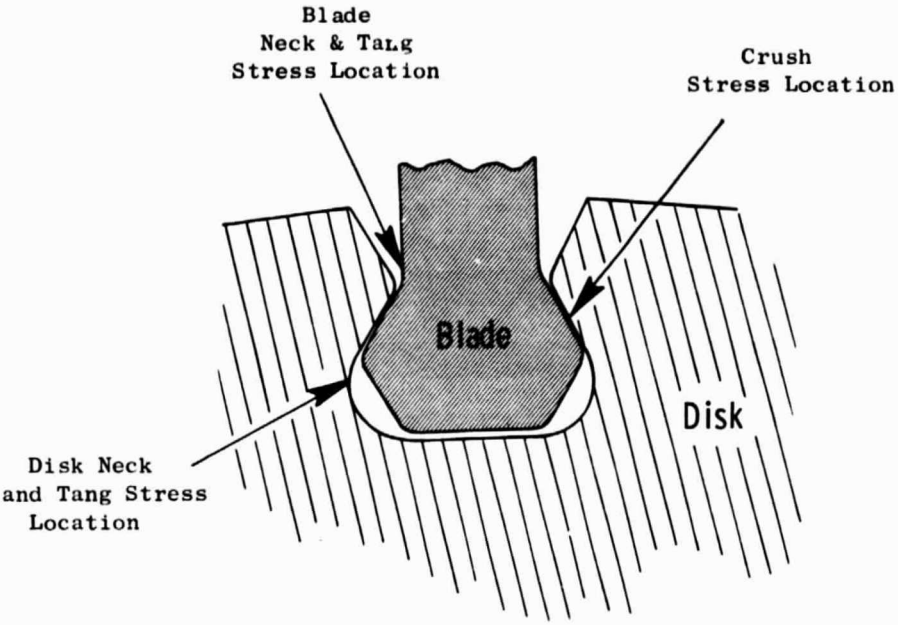

Dovetail Profile and Identification of Different Stress Locations

110% N_f = 11,692 rpm

Steady-State Dovetail Stresses

Blade Maximum Dovetail Stresses

Point	Combined	Neck	Tang	Crush
4	0.73 GN/m^2 (106 KSI)	0.46 GN/m^2 (67 KSI)	0.29 GN/m^2 (42 KSI)	0.41 GN/m^2 (60 KSI)

Disk Maximum Dovetail Stresses

Point	Combined	Neck	Tang	Crush
4	0.97 GN/m^2 (140 KSI)	0.71 GN/m^2 (102 KSI)	0.27 GN/m^2 (39 KSI)	0.41 GN/m^2 (60 KSI)

Figure 11. Location and Values of Calculated Dovetail Stresses, 110% Design Speed.

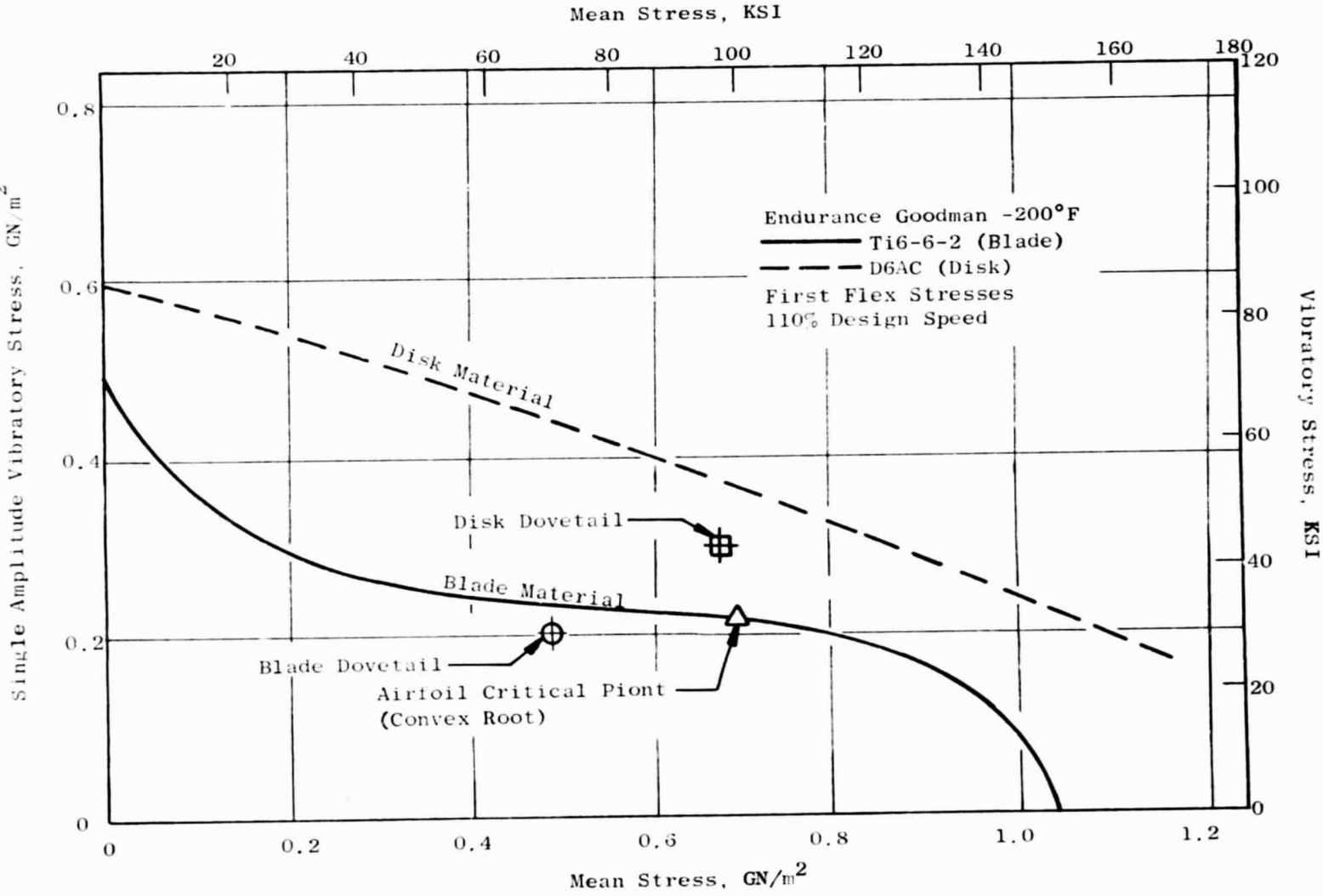

Figure 12. Relative Blade and Disc Dovetail Stress Levels with Airfoil Stressed to Vibratory Endurance Limit.

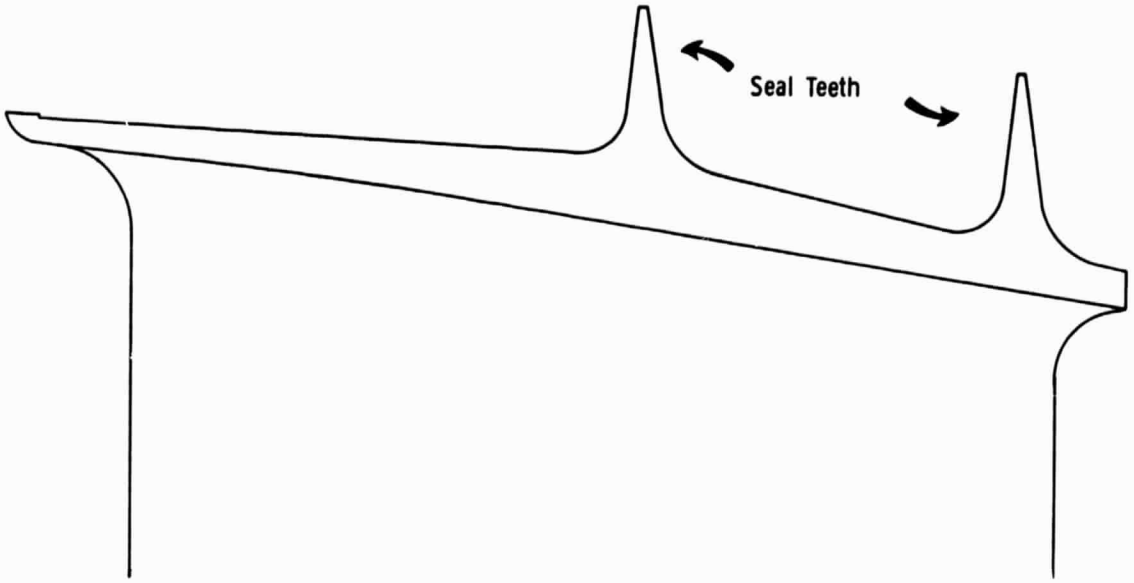

Figure 13. Tip Shroud Section (A-A of Figure 14).

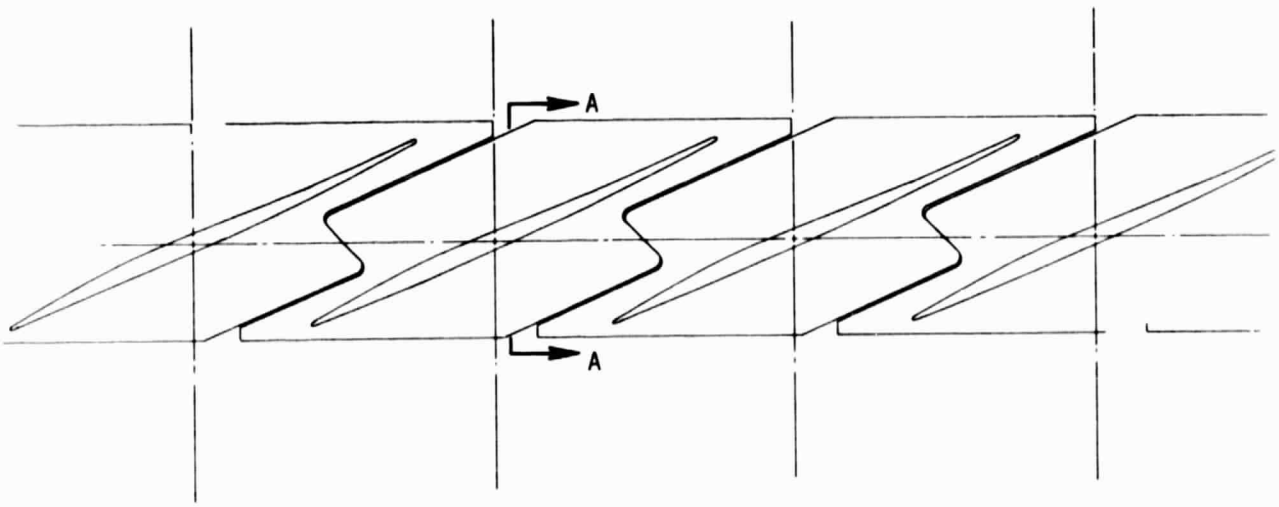

Figure 14. Tip Shroud Planform.

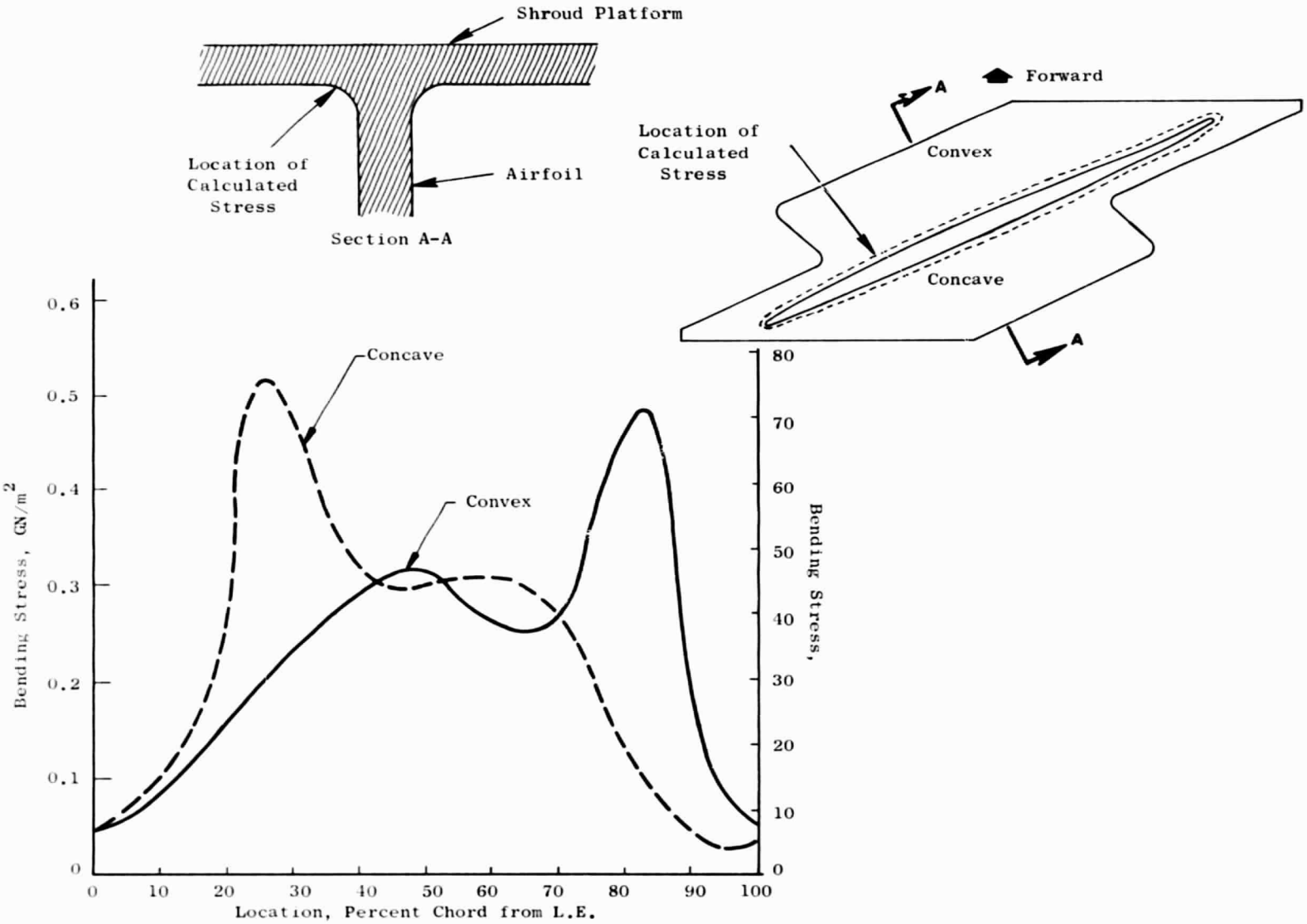

Figure 15. Tip Shroud Stress Distribution Along Airfoil Fillet, 100% Design Speed.

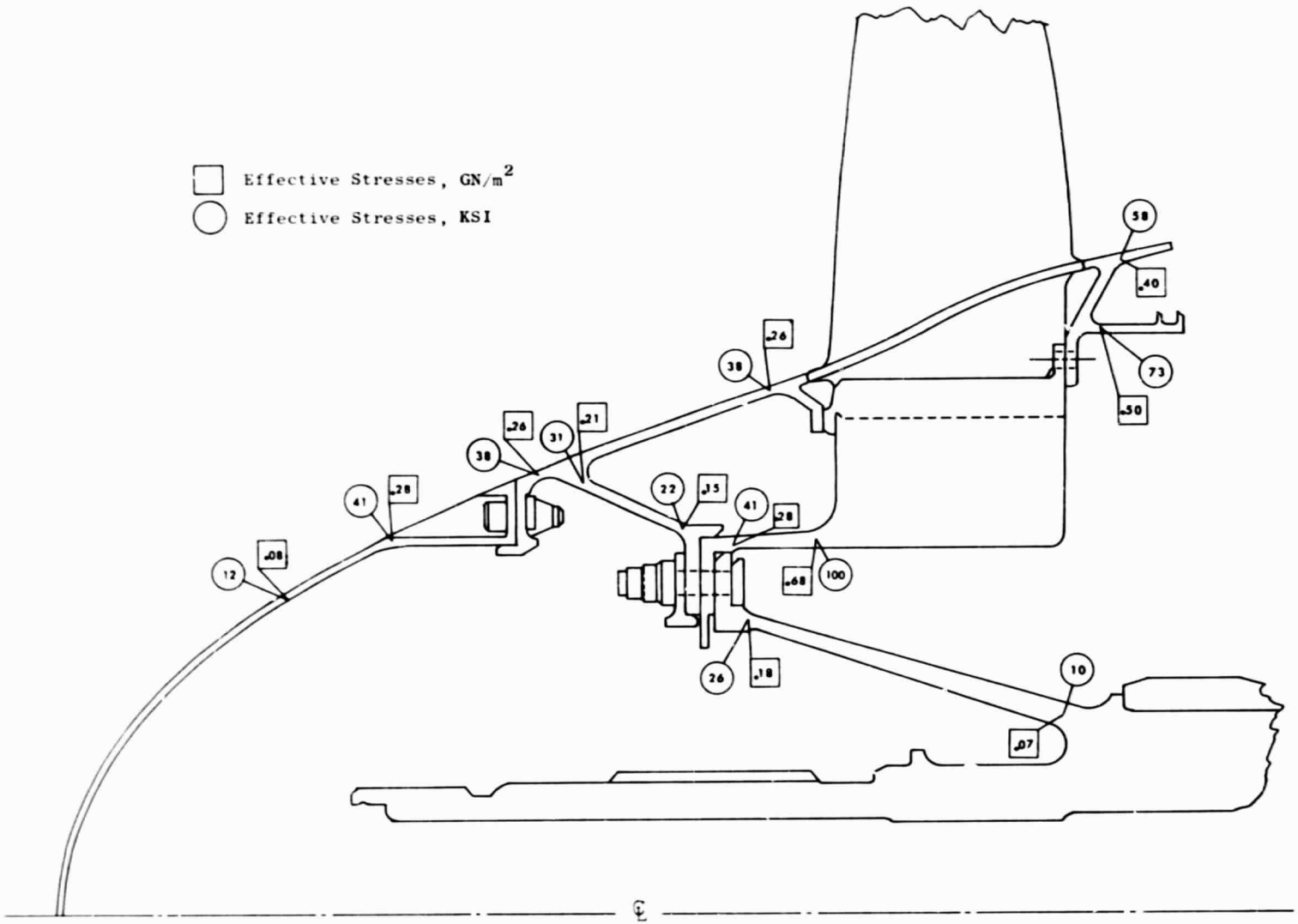

Figure 16. Fan Rotor Structure - Steady State Stresses, 100% Design Speed.

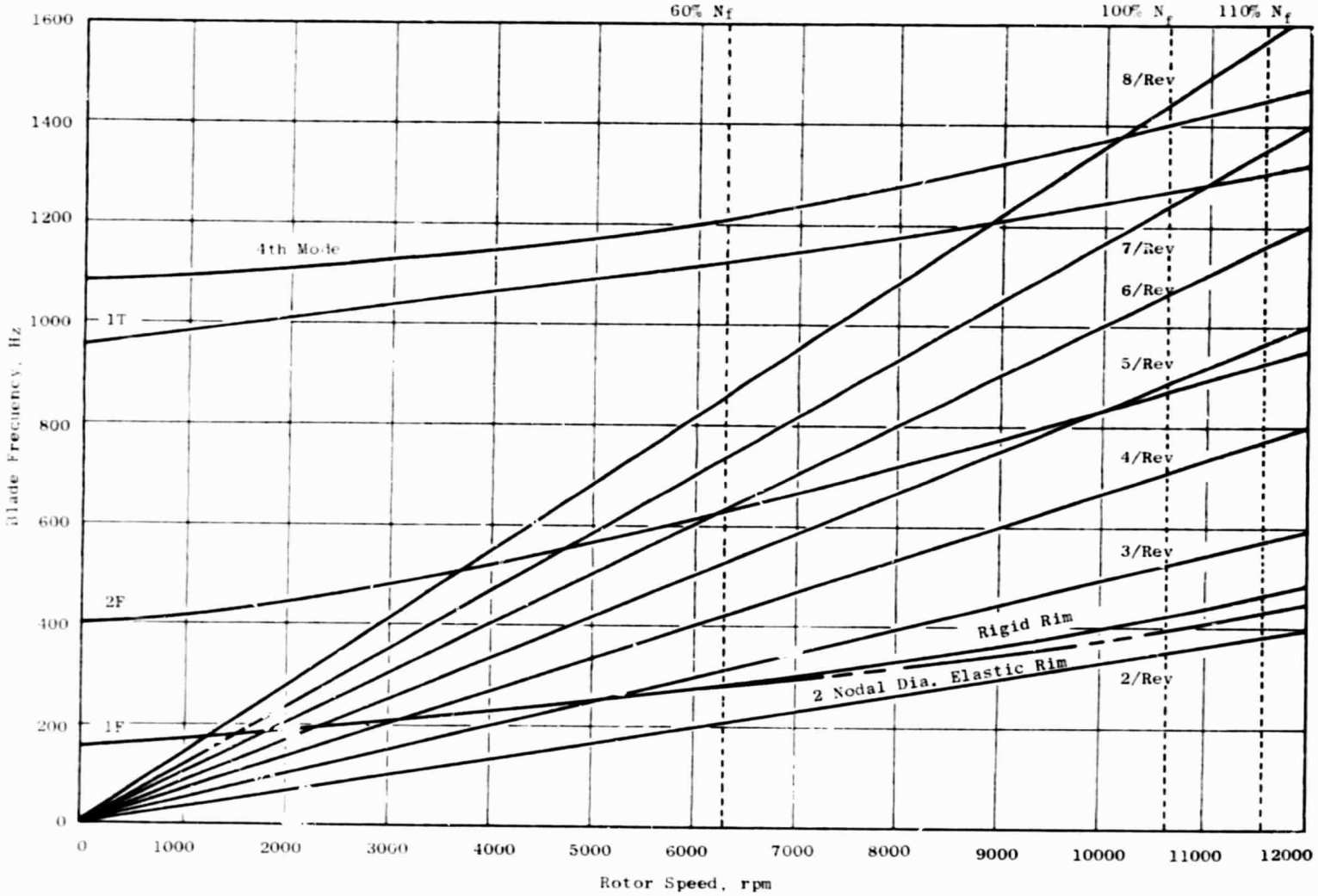

Figure 17. Fan Blade Campbell Diagram - Rotor Speed Vs. Blade Frequency.

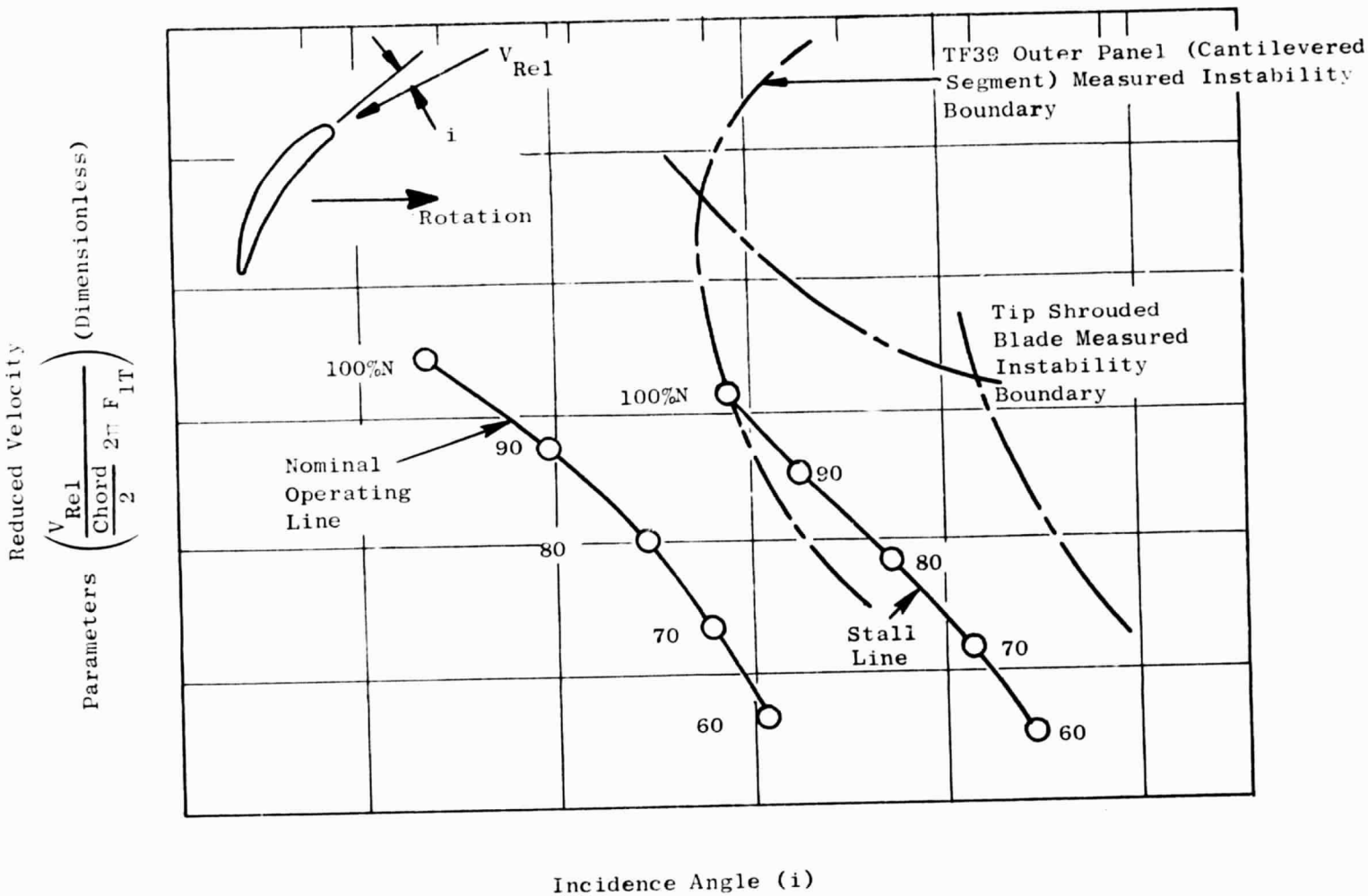

Figure 18. Fan Stability Plot Regions.

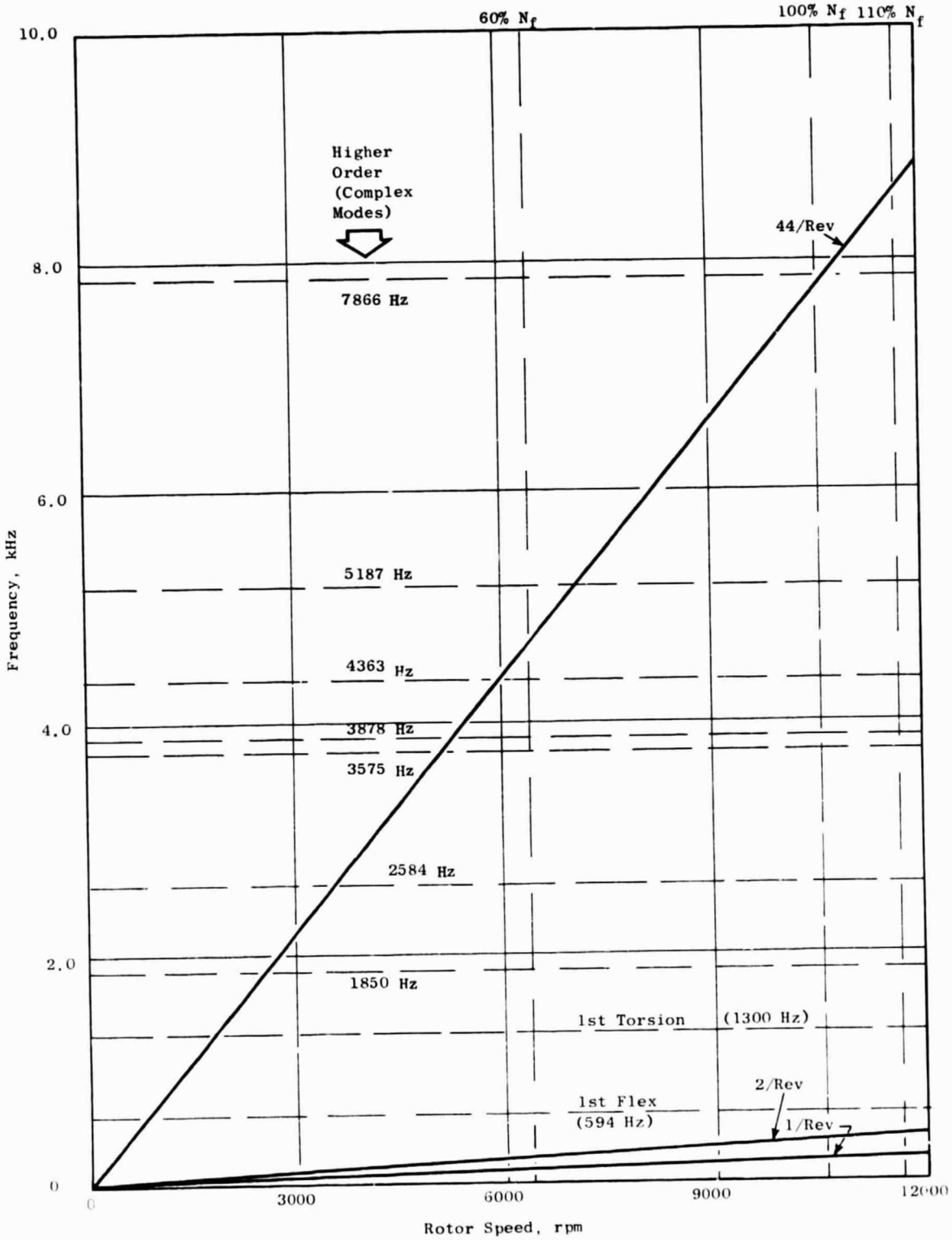

Figure 19. Bypass OGV Campbell Diagram.

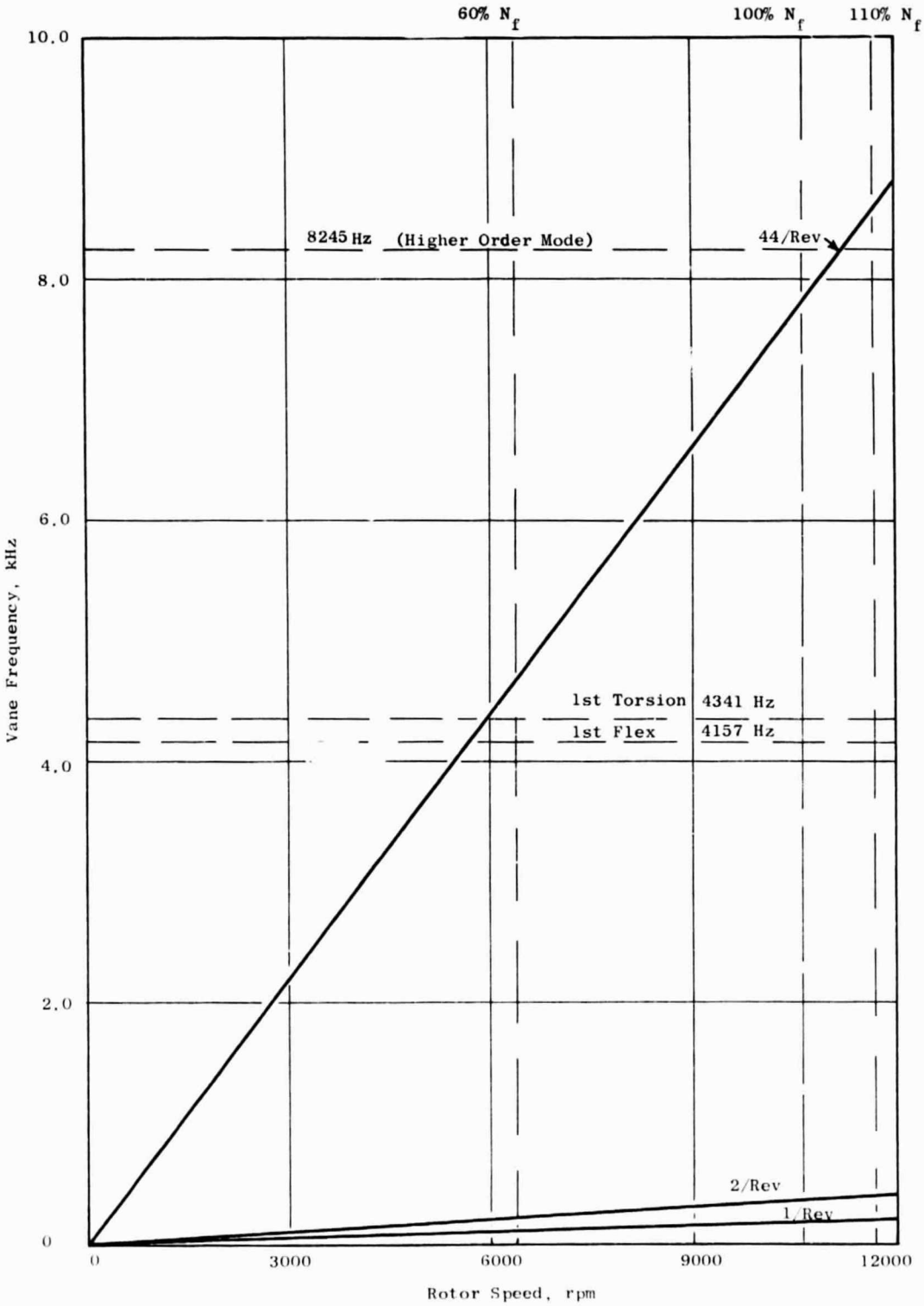

Figure 20. Core Stator Campbell Diagram.

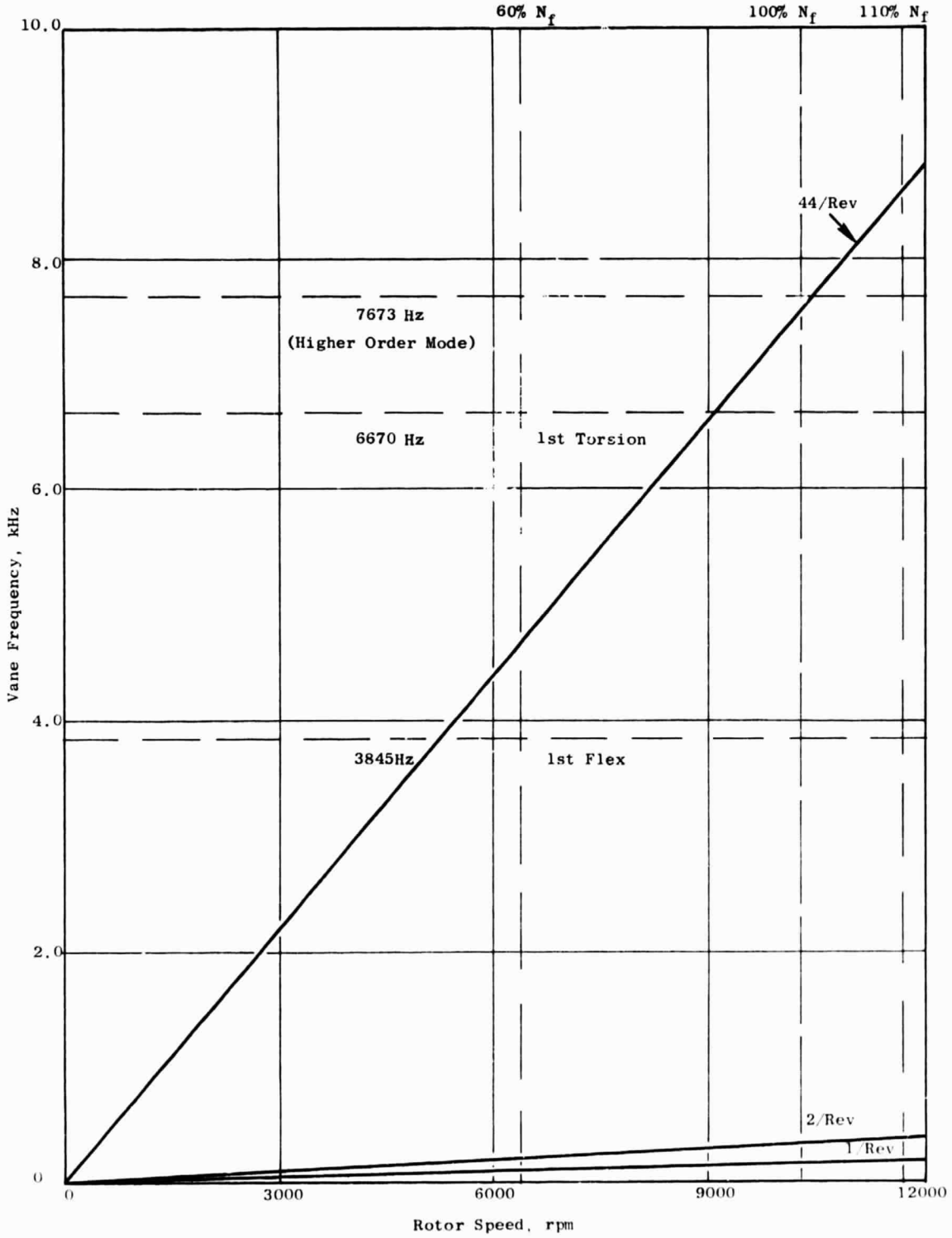

Figure 21. Deswirl Vane Campbell Diagram.

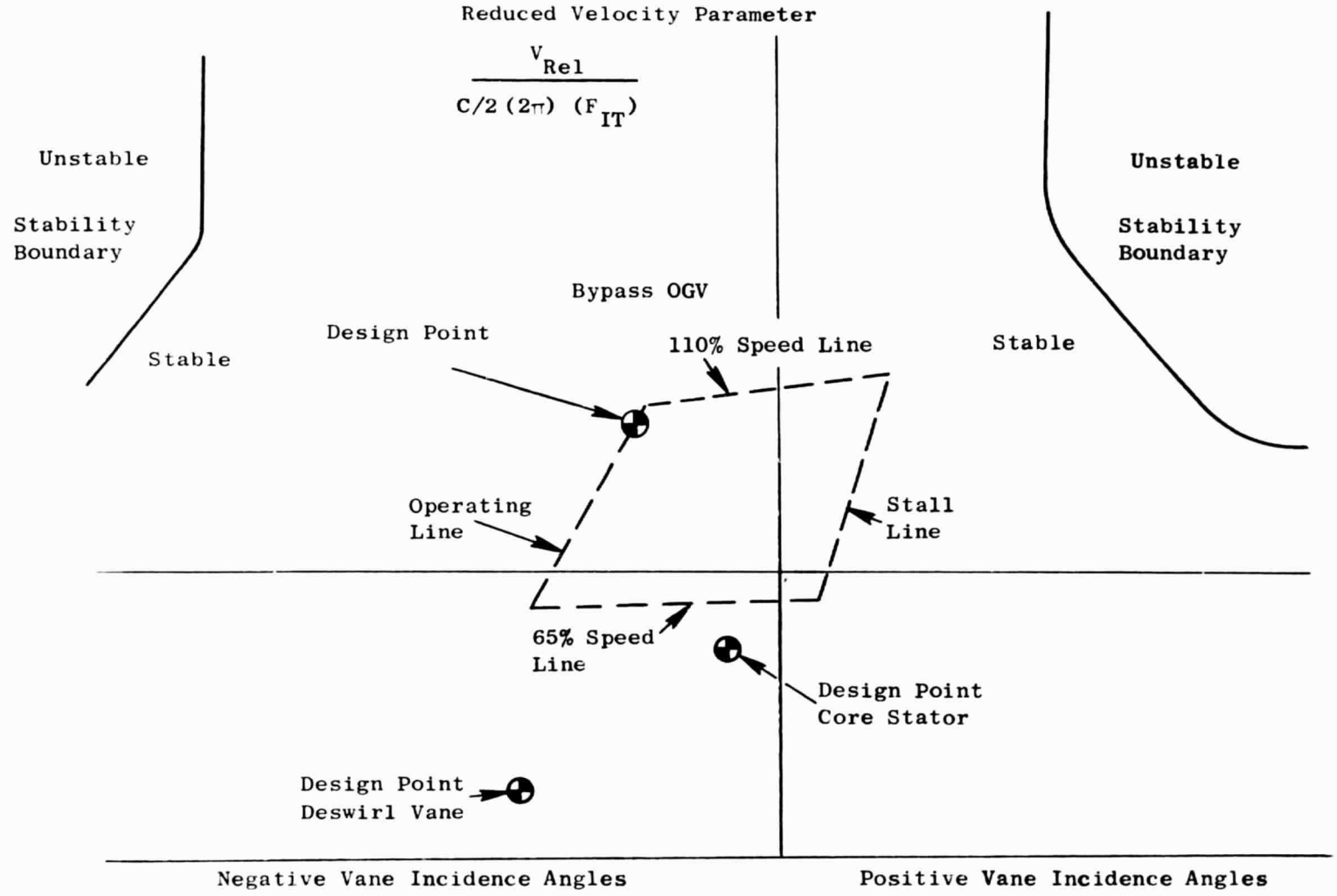

Figure 22. Torsional Stability Diagram.

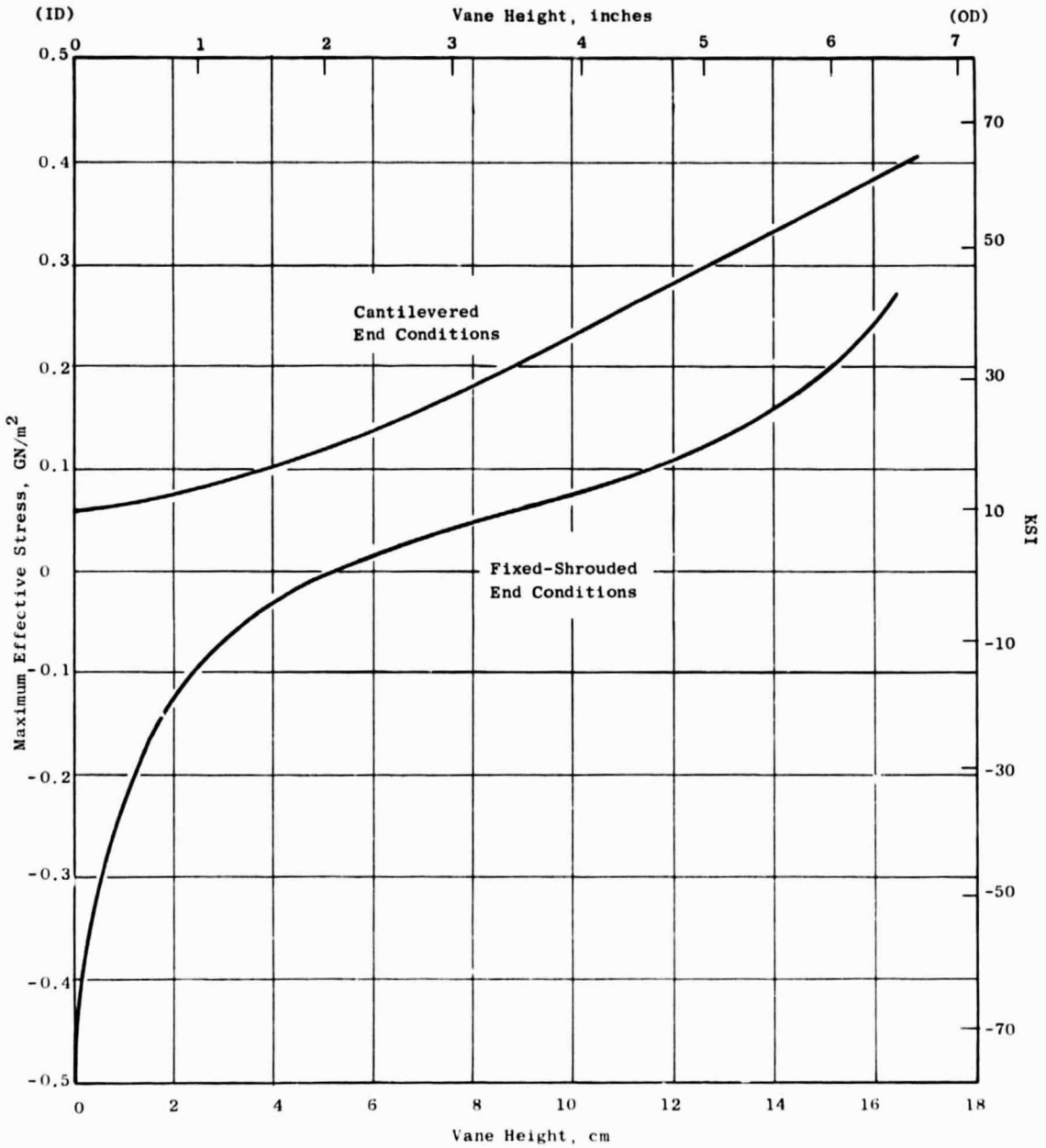

Figure 23. Bypass OGV Calculated Steady State Airfoil Stress Distribution Along the Trailing Edge Due to Air Loading at the 100% rpm Design Point.

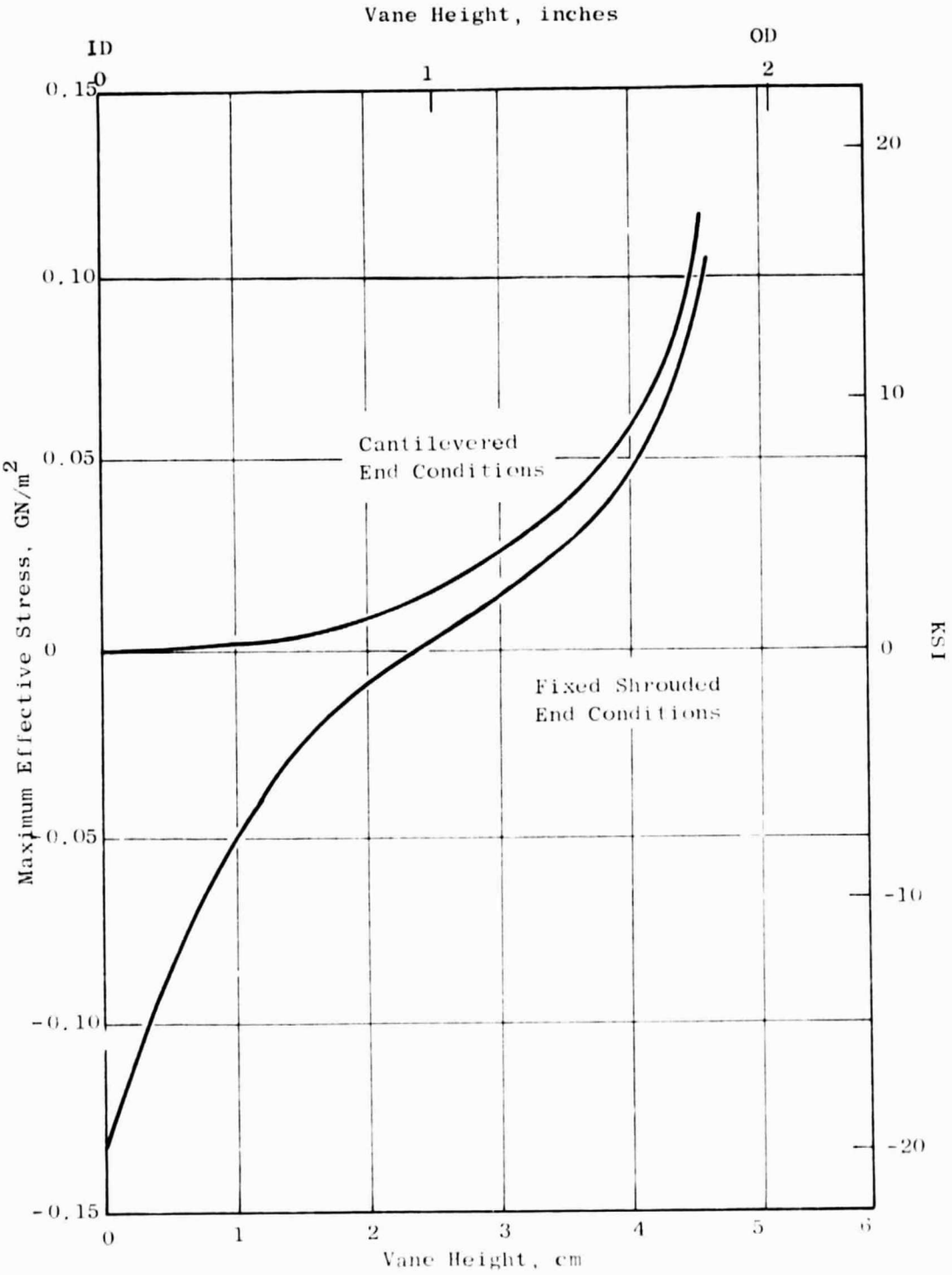

Figure 24. Core Stator Vane Calculated Steady State Airfoil Stress Distribution Along the Trailing Edge Due to Air Loading at the 100% rpm Design Point.

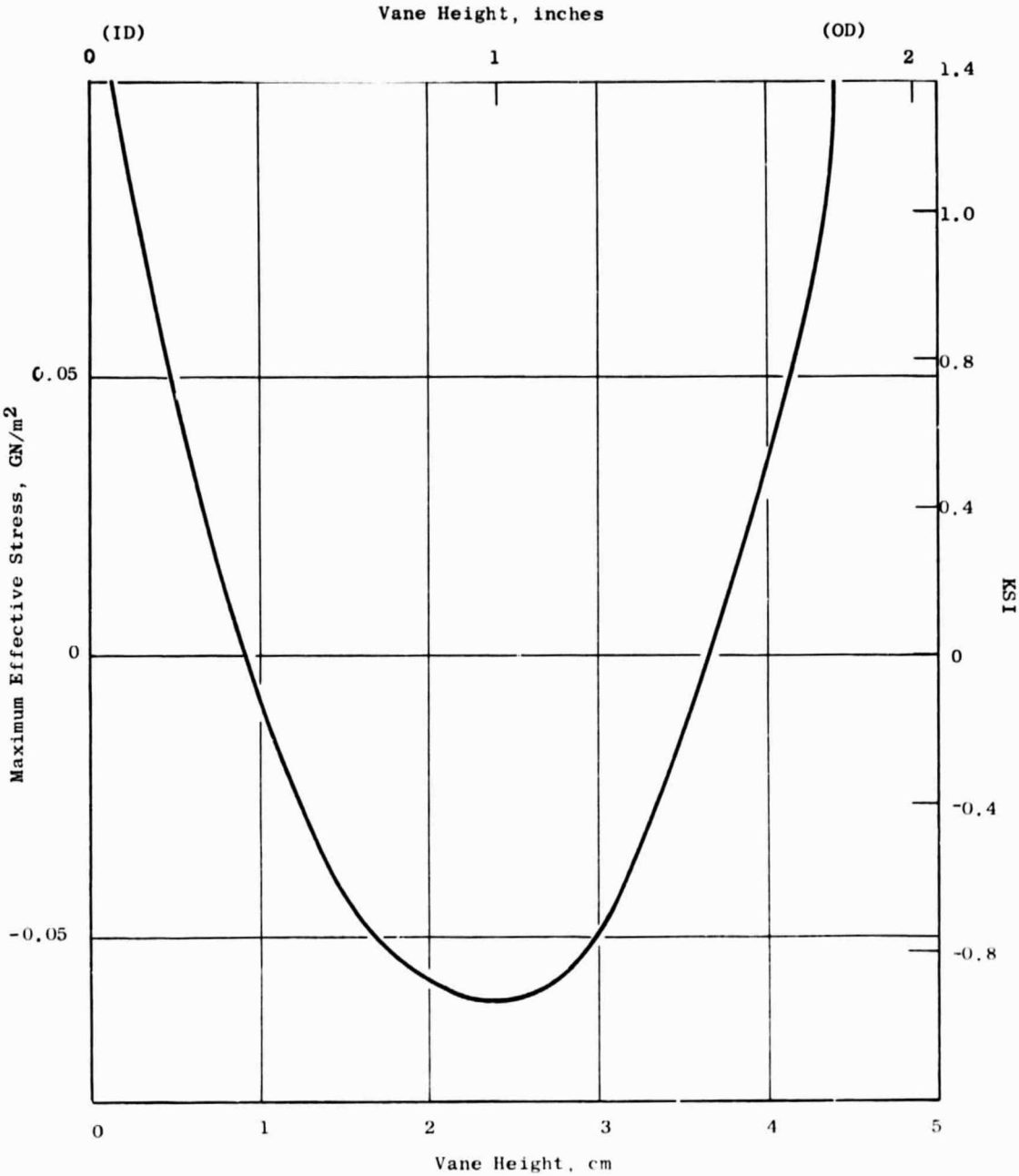

Figure 25. Deswirl Vane Calculated Steady State Airfoil Stress Distribution Along the Trailing Edge Due to Air Loading at the 100% rpm Design Point.

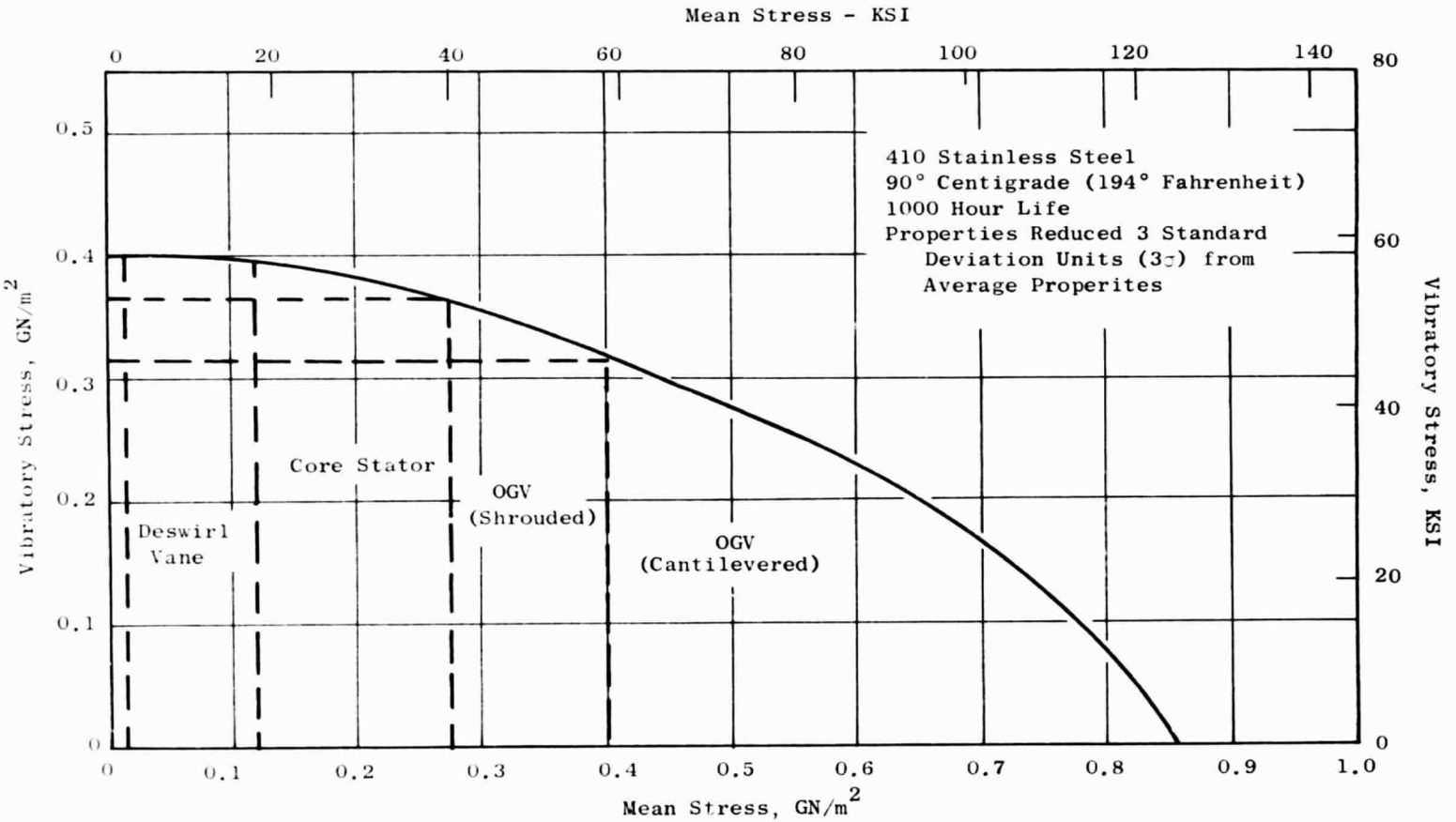

Figure 26. Resulting Vibratory Allowable Stress Based on Calculated Steady State Airfoil Stresses.